# MULTIELEMENT AEROFOILS WITH MOVING SURFACE BOUNDARY - LAYER CONTROL: WIND TUNNEL, NUMERICAL AND FLOW VISUALIZATION STUDIES

V.J. Modi[*], S.R. Munshi[**], F. Mokhtarian[***]
Department of Mechanical Engineering
University of British Columbia
Vancouver, B.C., Canada V6T 1Z4

G. Bandyopadhyay[+]
Department of Aerospace Engineering
Indian Institute of Technology
Kharagpur, W. Bengal, India 721302

and

T. Yokomizo[+]
Department of Mechanical Engineering
Kanto Gakuin University
Mutsuura, Kanazawa, Yokohama, Japan 326

## Abstract

The concept of Moving Surface Boundary-layer control (MSBC), as applied to a family of two-dimensional airfoils, is investigated through a planned wind tunnel test-program complemented by numerical and flow visualization studies. The moving surface was provided by rotating cylinder(s) located at the leading edge and/or trailing edge as well as the top surface of the airfoil. Results on the pressure distribution, lift and drag suggest that the concept is quite promising leading to a substantial increase in lift, reduction in drag, and a delay in the onset of stall. Depending on the performance desired, appropriate combinations of cylinder location and speed can be selected to obtain favourable results over a wide range of the angle of attack. Next, the system performance is predicted using two distinctly different numerical procedures which correlate with the experimental results well considering complex character of the flow.

*   Professor; Fellow AIAA, ASME
**  Graduate Research Assistant
*** Graduate Research Assistant, presently Staff
    Engineer, Canadair, Montreal, Quebec
+   Professor

A flow visualization study qualitatively substantiates the trends observed during the wind tunnel and numerical investigations. It shows, rather dramatically, effectiveness of the MSBC.

## Introduction

Ever since the introduction of boundary-layer concept by Prandtl, there has been a constant challenge faced by scientists and engineers to minimize its adverse effects and control it to advantage. Methods such as suction, blowing, vortex generators, turbulence promotors, etc. have been investigated at length and employed in practice with a varying degree of success. A vast body of literature accumulated over years has been reviewed rather effectively by several authors including Goldstein[1], Lachmann[2], Rosenhead[3], Schlicting[4], Chang[5] and others. However, the use of a moving wall for boundary-layer control has received relatively little attention as suggested by limited number of contributions in this area[6-9].

Irrespective of the method used, the main objective of a control procedure is to prevent, or at least delay, the separation of boundary-layer from the surface. A moving surface attempts to accomplish this

in two ways: it prevents the initial growth of boundary-layer by minimizing relative motion between the surface and the free stream; and it injects momentum into the existing boundary layer.

A practical application of the moving wall for boundary-layer control was demonstrated by Favre[10]. Using an airfoil with upper surface formed by a belt moving over two rollers, he was able to delay separation until the angle of attack reached 55° where the maximum lift coefficient of 3.5 was realized. Alvarez Calderon and Arnold[11] carried out tests on a rotating cylinder flap to develop a high lift airfoil for STOL type aircraft. The system was flight tested on a single engine high wing research aircraft.

Of some interest is the North American Rockwell's OV-10A which was flight tested by NASA's Ames Research Center [12-14]. Cylinders, located at the leading edge of the flaps, were made to rotate at high speed with the flaps in lowered position. The main objective of the test-programme was to assess handling qualities of the propeller-powered STOL-type aircraft at higher lift coefficients. The aircraft was flown at speeds of 29-31 m/s, along approaches up to -8°, which corresponded to the lift coefficient of about 4.3. In the pilot's opinion, any further reductions in the approach speed were limited by the lateral-directional stability and control characteristics.

The present study builds on this background and presents typical results obtained through a comprehensive investigation involving:

(i)  wind tunnel tests with a family of two dimensional airfoils;

(ii) numerical simulations; and

(iii) flow visualization studies;

in presence of the Moving Surface Boundary-layer Control (MSBC). As can be expected, the amount of information obtained through planned variations of the important parameters is literally enormous. Only a set of few typical results useful in establishing trends are presented here.

## Wind Tunnel Tests

### Models and Test Arrangement

Figure 1 shows a family of two-dimensional airfoils with different positions of the rotating elements used to inject momentum. Geometry of the airfoil (thickness ratio, cambre, etc.) were also varied. To provide flexibility in locating the cylinder on the airfoil and permit testing of multi-cylinder configurations, a sectional design was adopted. The model consists of an aluminum skin wrapped around an aluminum and steel frame with various sections of the surface removable, as required, to accommodate cylinders. A schematic diagram of the model in Figure 2 shows details of the construction, including the leading-edge rotating cylinder. A nose fill-in section replaced the leading edge cylinder when it was not used as a rotating element. The top panel was removed to house the upper-surface cylinders at locations shown in Figure 1. The rotating cylinders were mounted between high-speed bearings housed in the brackets at either end of the model. They were driven by 1/4 hp, 3.8 A variable speed motors, located outside the tunnel, through standard couplings.

The model was provided with a total of 44 pressure taps, distributed over the circumference, to yield detailed information about the surface loading. However, once a section of the model was removed to accommodate a cylinder, the pressure taps in that section were lost. Although the pressure information over the small region represented by the upper-surface cylinder is not of particular significance, the corresponding data at the leading edge of the airfoil is crucial since it represents a high-suction region. Its measurement presented a challenging task. Locating pressure taps on the surface of the cylinder, typically rotating in the range of 2000-8000 rpm, offers considerable practical difficulty. The problem was resolved by measuring the pressure in the immediate vicinity of the cylinder rather than on the surface itself.

The wind tunnel model, approximately 0.38 m along the chord and 0.68 m long, spanned the tunnel test-section, 0.91 x 0.68 x 2.6m, to create essentially two-dimensional condition. It was supported by an Aerolab six-component strain gauge balance and tested in a low-speed, low-turbulence return-type wind tunnel where the airspeed can be varied from 1-50 m/s with a turbulence level of less than 0.1%. A Betz micromanometer with an accuracy of 0.2 mm of water was used to measure pressure differential across the contraction section of 7:1 ratio. The rectangular test-section (0.91 x 0.68 m) is provided with 45° corner fillets that vary from 15.25 x 15.25 to 12 x 12 cm to partly compensate for the boundary-layer growth. The spatial variation of velocity in the test-section is less than 0.25%.

The tests were conducted over an extended range of the angle of attack $\alpha$ and cylinder rotational speeds, corresponding to $U_c/U$ = 0,1,2,3,4 at a Reynolds number (Re) of 4.62 x $10^4$ ($U_c$ = cylinder surface velocity; U = free stream velocity; Re based on U and the chord). The choice of the Reynolds number in this case was dictated by vibration problems with multicylinder configurations operating at high rotational speeds (around 8000 rpm for $U_c/U$ = 4). The
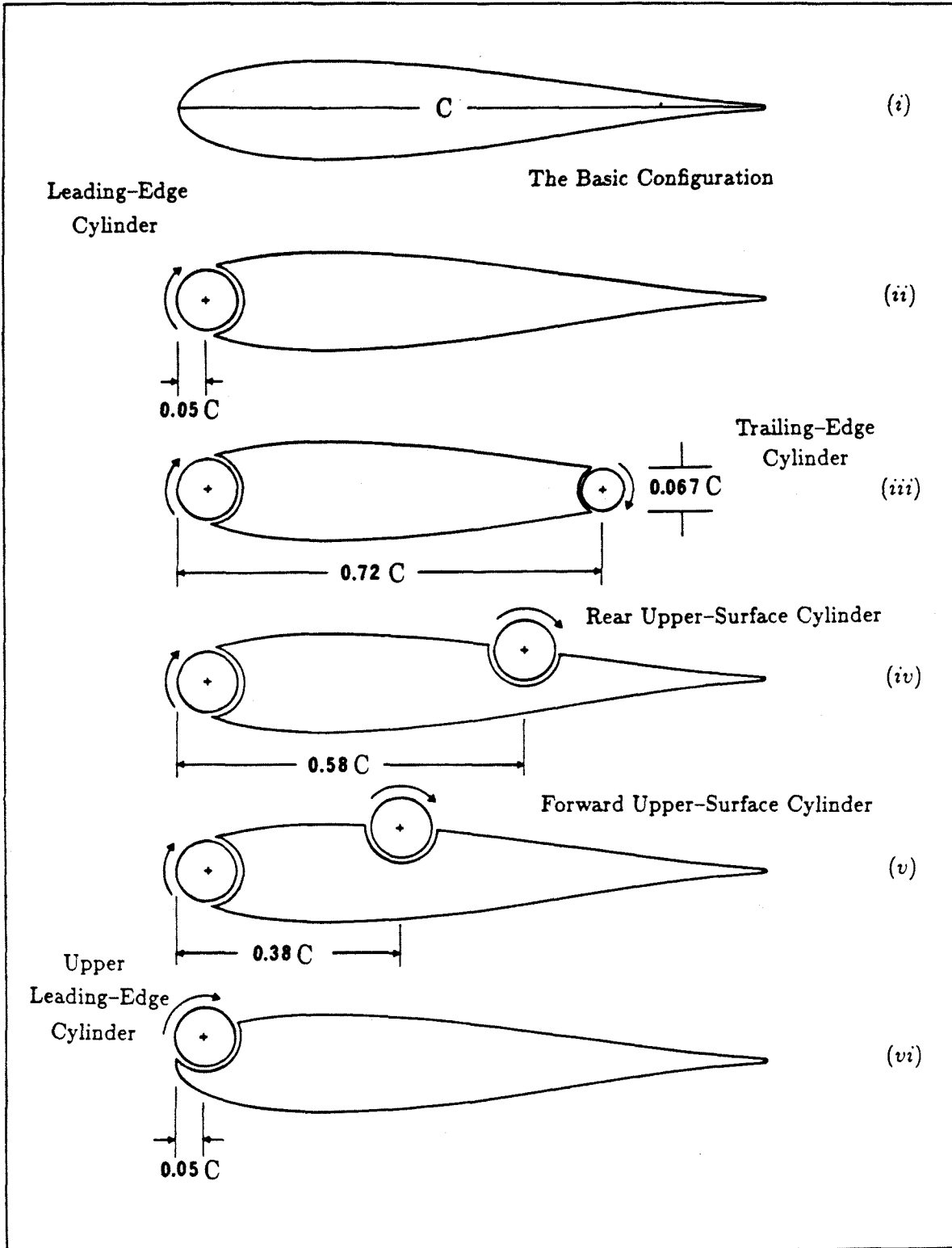
Figure 1    Various rotating-cylinder configurations studies with the Joukowsky airfoil model.

pressure plots were integrated in each case to obtain the lift coefficient.

The lift was also measured independently using the Aerolab balance to assess two-dimensional character of the flow. To that end, the model was mounted with its spanwise axis perpendicular to the supporting platform of the balance and the wall clearance at either end of the model was kept to a minimum (less than 3 mm). The tests were carried out at several angles of attack and cylinder rotational speeds. The cylinder rotation introduced high-frequency modulations to the force signal, which were eliminated using a band-pass filter. The force data correlated remarkably well with the pressure integrated values. The difference between the two depended on $\alpha$ and $U_C/U$ but was never more than 4%, the estimated error range of the measuring instrumentation.

The configurations tested include the leading-edge cylinder (l.e.), trailing-edge cylinder (t.e.), forward upper-surface cylinder ($f$), rear upper-surface cylinder ($r$), leading-edge and upper-surface cylinders, and upper leading-edge cylinder (u.l.e.).

## Results and Discussion

The relatively large angles of attack used in the experiments result in a considerable blockage of the wind-tunnel test-section, from 21% at $\alpha = 30°$ to 30% at $\alpha = 45°$. The wall confinement leads to an increase in local wind speed at the location of the model, thus resulting in an increase in aerodynamic forces. Several approximate correction procedures have been reported in literature to account for this effect. However, these procedures are mostly applicable to streamlined bodies with attached flow. A satisfactory procedure applicable to a bluff body offering a large blockage in a flow with separating shear layers is still not available.

With rotation of the cylinder(s), the problem is further complicated. As shown by the pressure data and confirmed by the flow visualization, the unsteady flow can be separating and reattaching over a large portion of the top surface. In absence of any reliable procedure to account for wall confinement effects in the present situation, the results are purposely presented in the uncorrected form, unless specified otherwise.

## Base Airfoil

The pressure distribution data for the "base airfoil" (in absence of the modifications imposed by the leading-edge or upper-surface cylinder) are presented in Figure 3. The leading edge was now formed by a snugly fitting plug (the nose fill-in section). Due to practical difficulty in locating pressure taps in the cusp region, there is an apparent discontinuity in the pressure plots near the trailing edge. However, this region has little importance in the present discussion. It is apparent that the airfoil, in absence of any modifications to its nose geometry, stalls at an angle of attack of around 10-12°. These results serve as reference to assess the effect of rotating cylinders in different locations.

Note that the wall confinement effect at $\alpha = 10°$ is relatively small, as the blockage ratio is around 7%. More importantly, focus here is on the effect of the momentum injection due to the cylinder rotation with the airfoil at a given angle of attack. Results of the flow visualization study, presented later, emphasize this point.

## Leading Edge Cylinder

Figure 4 summarizes the effects of modification of the airfoil with the leading-edge cylinder and the cylinder rotation. The base airfoil has a maximum lift coefficient of about 0.87 at an angle of attack of 10°. There is a penalty associated with the modified nose geometry as well as due to the gap, but even at the lowest rate of rotation of the cylinder ($U_C/U = 1$) the lift and stall characteristics are significantly improved. The airfoil exhibits a desirable flattening of the lift curve at stall. The maximum lift coefficient measured with $U_C/U = 4$ was around 2 at $\alpha = 28°$, which is almost three times the lift coefficient of the base airfoil.

Typical pressure plots at a relatively larger angle of attack are presented in Figure 5 to assist in more careful examination of the local flowfield. As the angle of attack of the airfoil is increased, the flow starts to separate from the upper surface close to the leading edge. At $\alpha = 16°$, for example, the cylinder rotating at $U_C/U = 1$ only keeps the flow attached at the leading edge. However, as the rate of rotation is increased, the size of the separated region is reduced, and at the higher rate of rotation the flow is again completely attached. Note that the point of separation on the upper surface clearly moves downstream with an increasing rate of rotation. The flow separates at around X/C = 25% with $U_C/U = 2$, around X/C = 80% when $U_C/U$ is increased to three, and at the trailing edge with the
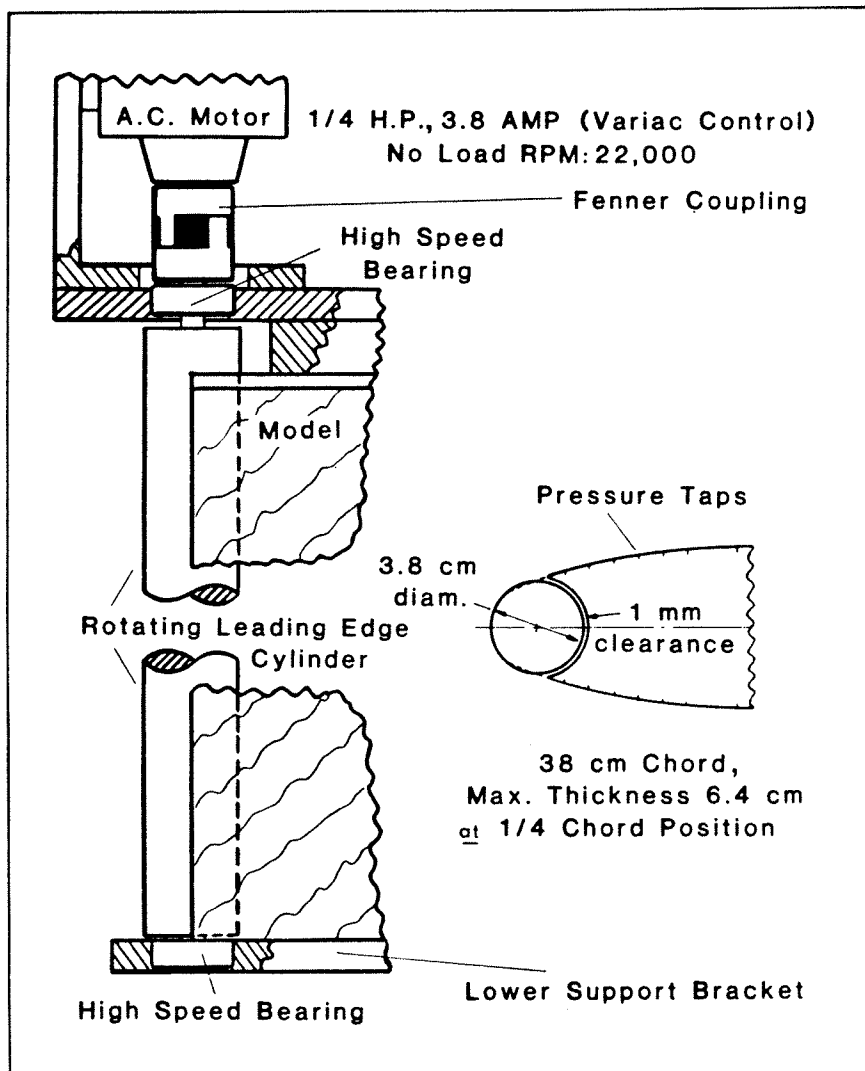
A.C. Motor  1/4 H.P., 3.8 AMP (Variac Control)
No Load RPM: 22,000

Fenner Coupling

High Speed
Bearing

Model

Pressure Taps

3.8 cm
diam.

1 mm
clearance

Rotating Leading Edge
Cylinder

38 cm Chord,
Max. Thickness 6.4 cm
at 1/4 Chord Position

High Speed Bearing

Lower Support Bracket

Figure 2    Detailed schematic of the leading-edge rotating cylinder
and cylinder-drive mechanism.

Joukowsky

- $\alpha = 0°$
- $\alpha = 4°$
- $\alpha = 8°$
- $\alpha = 10°$
- $\alpha = 12°$

$C_P$

$X/C$

$Re = 4.62 \times 10^4$
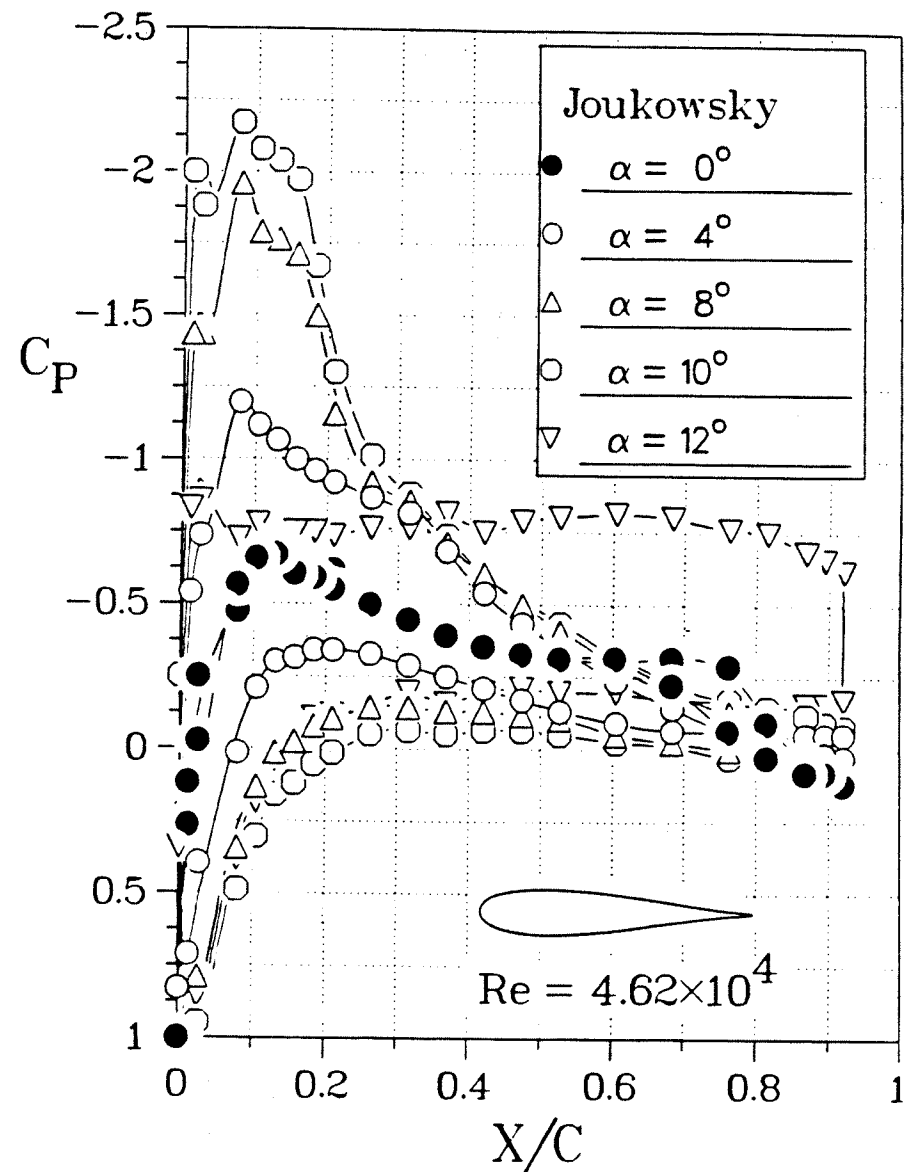
Figure 3    Experimentally obtained pressure distributions for the
basic Joukowsky model.
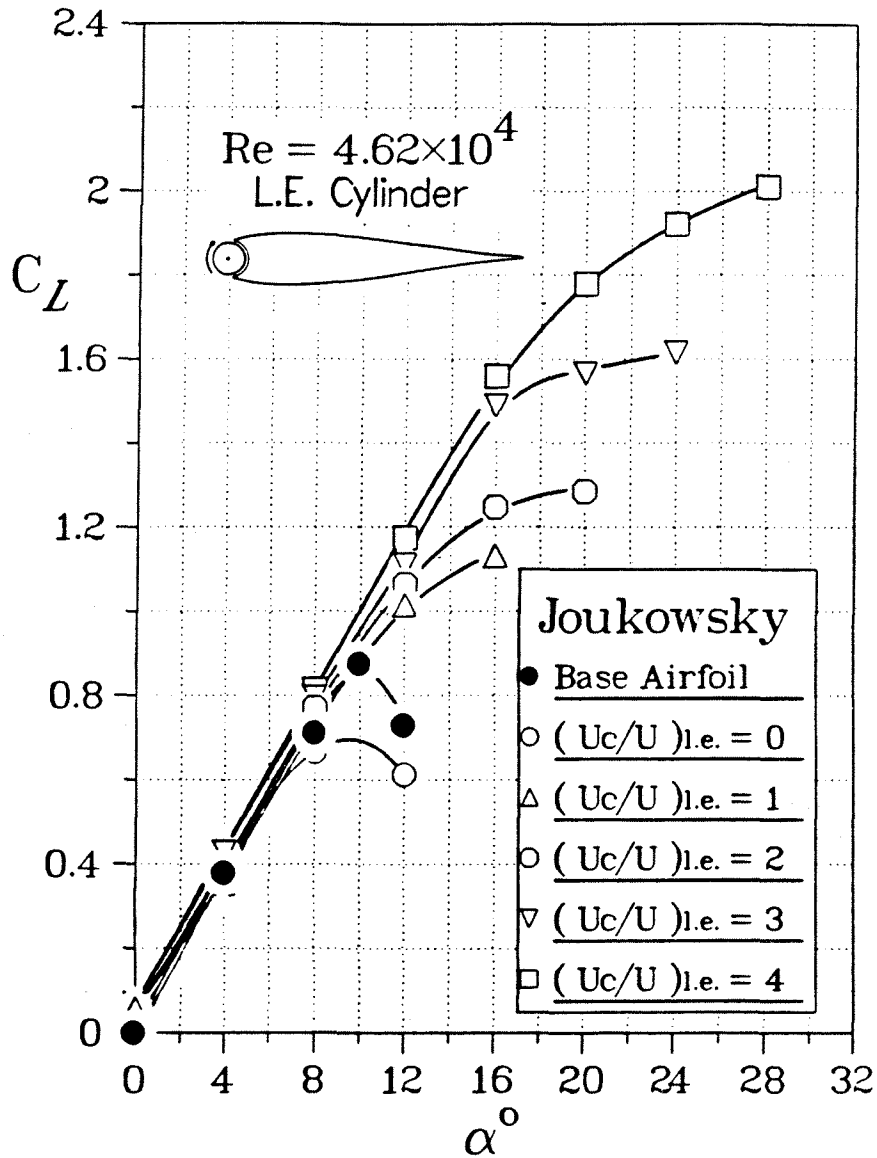
Figure 4    Effect of the leading-edge cylinder rotation on the lift and stall characteristics of the Joukowsky model.
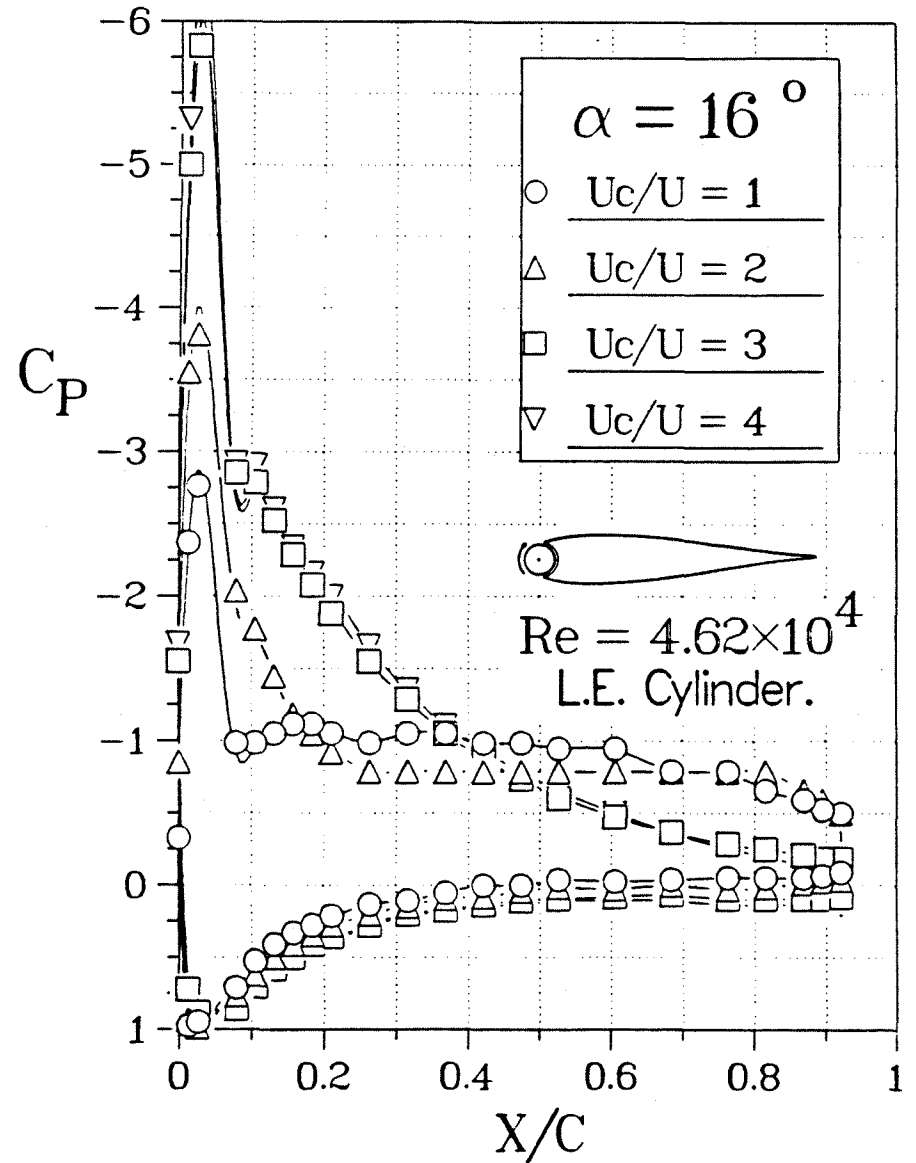


Figure 5    Effect of increasing the rate of cylinder rotation on pressure distribution around the model at relatively larger angles of attack of $\alpha = 16°$.

highest $U_c/U$ used. The flow visualization study discussed later substantiated this general behaviour rather dramatically.

## Trailing Edge Cylinder

The model was next tested with the trailing-edge cylinder. Unlike the leading-edge configuration, the cylinder at the trailing edge changes the basic geometry substantially. The trailing edge of the airfoil beyond $\approx 72\%$ chord is removed to accommodate the cylinder. The resulting chord is approximately 28% shorter than that of the base airfoil, and the model has a blunt trailing edge in the form of a cylinder.

A representative set of pressure plots for this model are presented in Figure 6. In absence of the cylinder rotation, the pressure distribution over the airfoil is not changed substantially compared to that for the model with the trailing edge. With rotation of the trailing-edge cylinder, both the suction over the upper surface and the compression on the lower surface increase. The effect is particularly noticeable with the higher rate of cylinder rotation and at the lower angle of attack (Figure 6a). The relative improvement decreases at the larger angle but is still quite evident near the stall (Figure 6b). This, in turn, results in a large improvement in the lift coefficient, as shown in Figure 7. For example, rotating the trailing-edge cylinder at $U_c/U = 4$ results in an increase in lift by about 320% at $\alpha = 4°$ (about 130% at $\alpha = 8°$). In contrast to the leading-edge cylinder, however, this configuration does not extend the stall beyond that of the base configuration. As can be expected, the trailing-edge cylinder essentially behaves as a flap shifting the plots to the left.

## Combined Leading and Trailing Edge Cylinders

The use of a leading-edge cylinder extends the lift curve, thus substantially increasing the maximum lift coefficient and delaying stall. On the other hand, the trailing-edge cylinder rotation results in an improvement in the lift coefficient, at a given angle of attack, before stall. In order to combine these effects, the base configuration was modified to include both the leading and trailing-edge cylinders. This phase of the test-program examined the effect of individual and combined cylinder rotations. However, it is the combined effects of both the cylinders that is of interest here. Results shown in Figure 8 suggest some benefit due to rotation of the two cylinders together. Although the increase in $C_{L,max}$ is rather modest (from 1.75 to 2.2, around 27%) compared to the leading-edge cylinder case (sharp trailing edge), the lift coefficient at a given $\alpha$ is indeed increased significantly, as expected,

due to the leftward shift of the plots. As noted before, this is due to the added circulation contributed by the trailing-edge cylinder. For example, $C_L = 0.8$ at $\alpha = 8°$ and $(U_c/U)_{l.e.} = 3$, whereas for the same angle of attack and $(U_c/U)_{l.e.} = (U_c/U)_{t.e.} = 3$ the corresponding $C_L \approx 1.57$, an increase of around 96%. Similarly, $C_L \approx 1.45$ for $\alpha = 16°$ and $(U_c/U)_{l.e.} = 4$. On the other hand, with both the cylinders rotating at $U_c/U = 4$, the lift coefficient is around 2.15, a further gain of about 50%. Note, the maximum life coefficient attained with rotation of both the cylinders represents an increase of 160% with respect to the reference configuration ($C_{L,max}$ of about 2.22 vs 0.88, Figure 8).

## Forward and Rear Upper Surface Cylinders

The forward and rear upper-surface cylinders, located at 38% and 58% chord, respectively, were considered independently and with either operating in conjunction with the leading-edge cylinder. As can be expected, in absence of rotation, their protrusion into the upper-surface flow had an adverse effect on the aerodynamic characteristics of the model. The flow separated at the location of the cylinder, resulting in a lower lift and increased drag. On the other hand, with rotation, either of the upper-surface cylinders was successful in attaining a higher $C_{L,max}$ and delaying the stall. In this respect, the forward upper-surface cylinder was particularly effective.

## Upper Leading Edge Cylinder

Effectiveness of the combination of leading-edge and forward upper-surface cylinders suggested a possibility of replacing the two by a single cylinder. This avoids the practical complications associated with construction, installation and operation of two rotating cylinders.

The configuration, with a cylinder located at approximately 5% of the chord, was tested at cylinder speeds in the range of $U_c/U$ up to 4. The results are presented in Figure 9. Compared to the leading edge cylinder study (Figure 4), where for $U_c/U = 4$, $C_{L,max} \approx 2$ and $\alpha_{stall} \approx 28°$, now we have $C_{L,max} \approx 2.35$ with $\alpha_{stall} \approx 48°$. This clearly suggests that location of the cylinder near the leading edge can significantly affect the airfoil performance. Thus, there is room for a systematic study to arrive at an optimum location. Even compared to the results obtained using the leading-edge cylinder together with the forward upper-surface cylinder, performance of the present single cylinder configuration appears attractive. Although the $C_{L,max}$ is slightly lower (down from 2.73 to 2.35), the stall is delayed from around 40 to 48°. However, the main
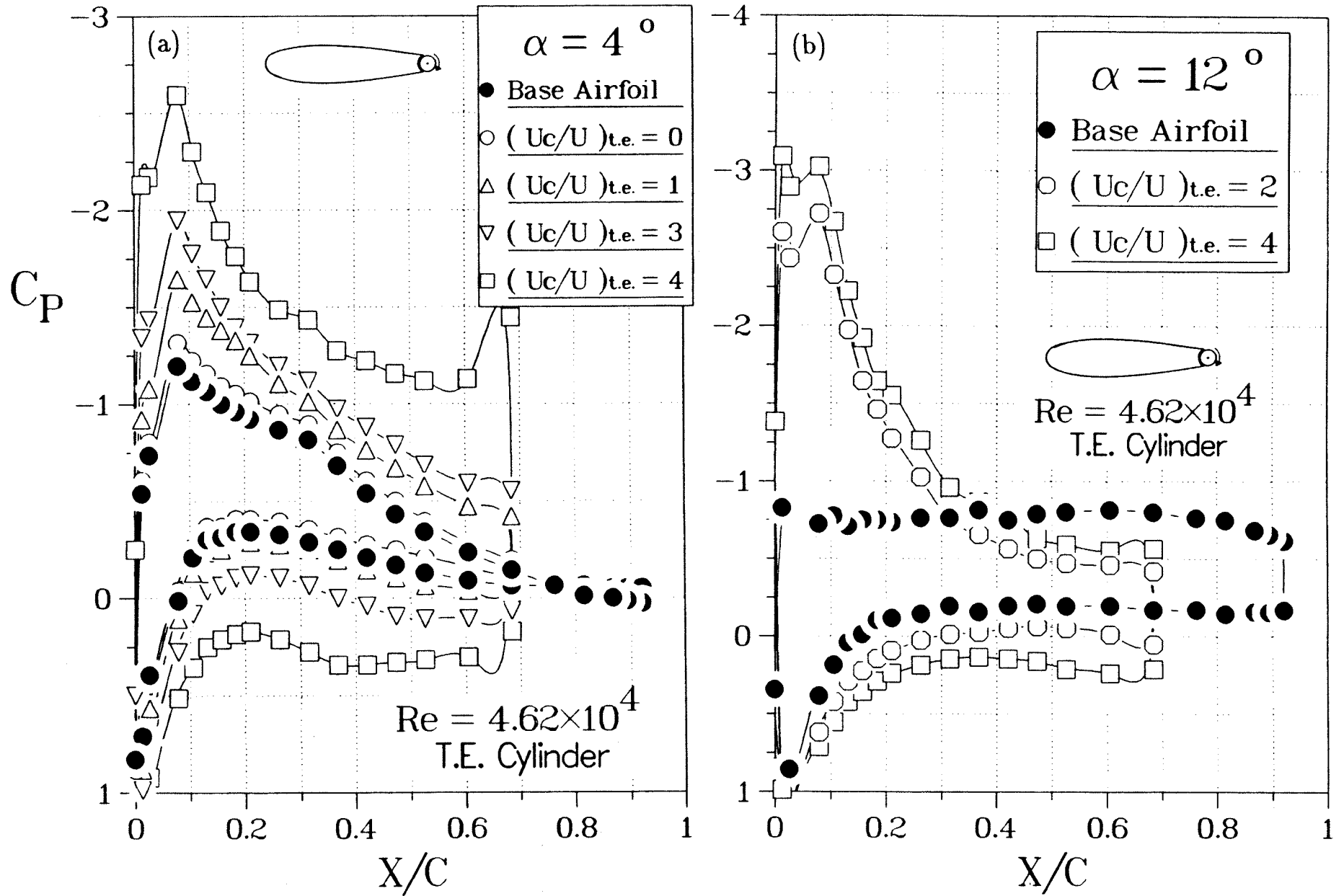
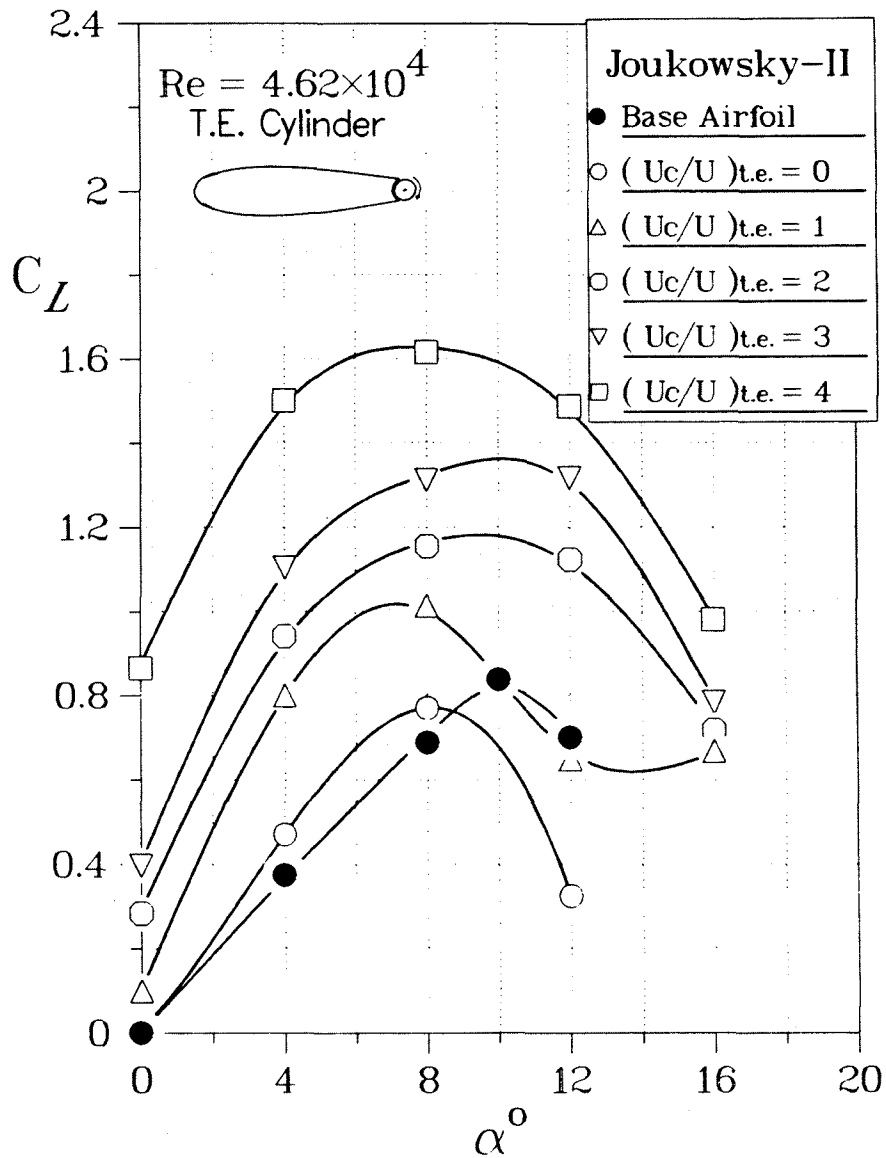Figure 6     Pressure distributions over the Joukowsky model modified with a trailing-edge cylinder.

Figure 7    Effect of the trailing-edge cylinder rotation on the lift and stall charactertistics of the Joukowsky model.
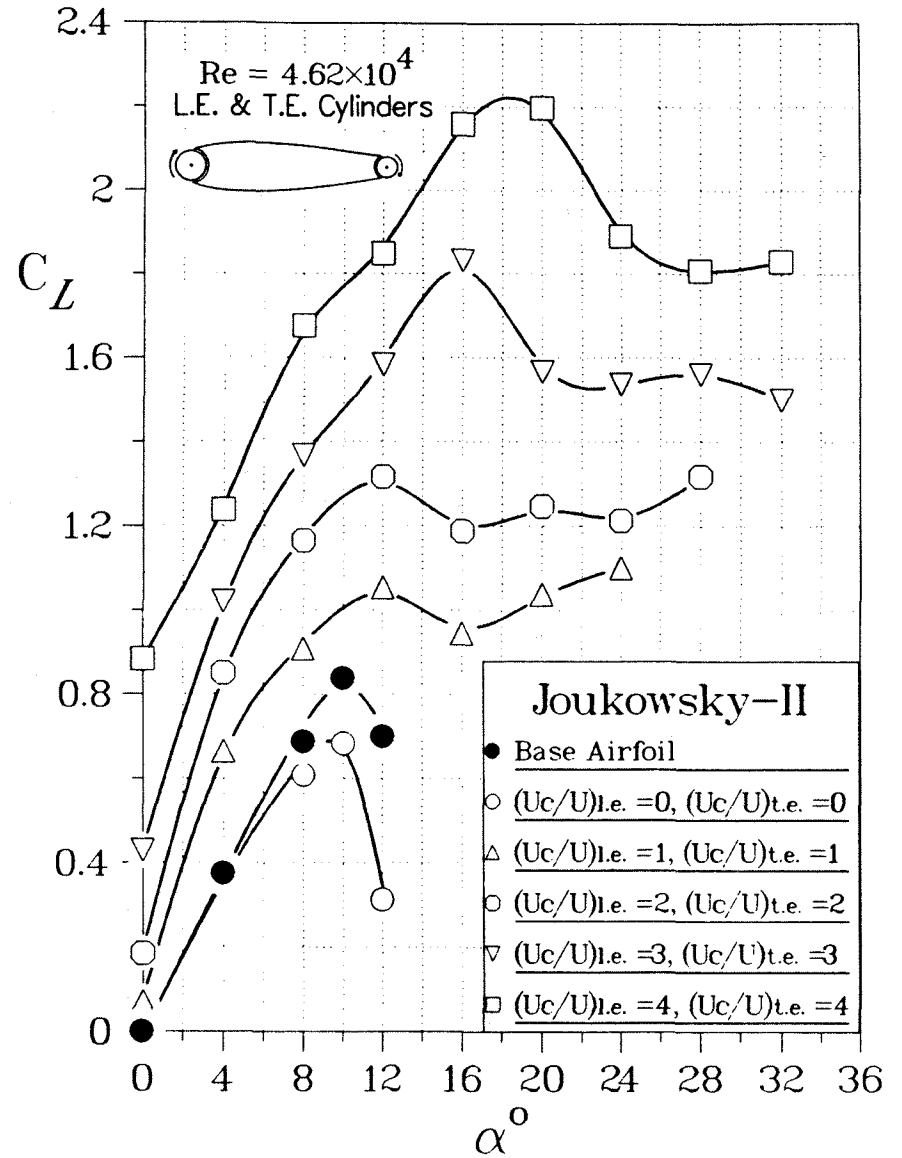
Figure 8    Variation of $C_L$ vs $\alpha$ for a modified Joukowsky airfoil with leading and trailing-edge cylinders.
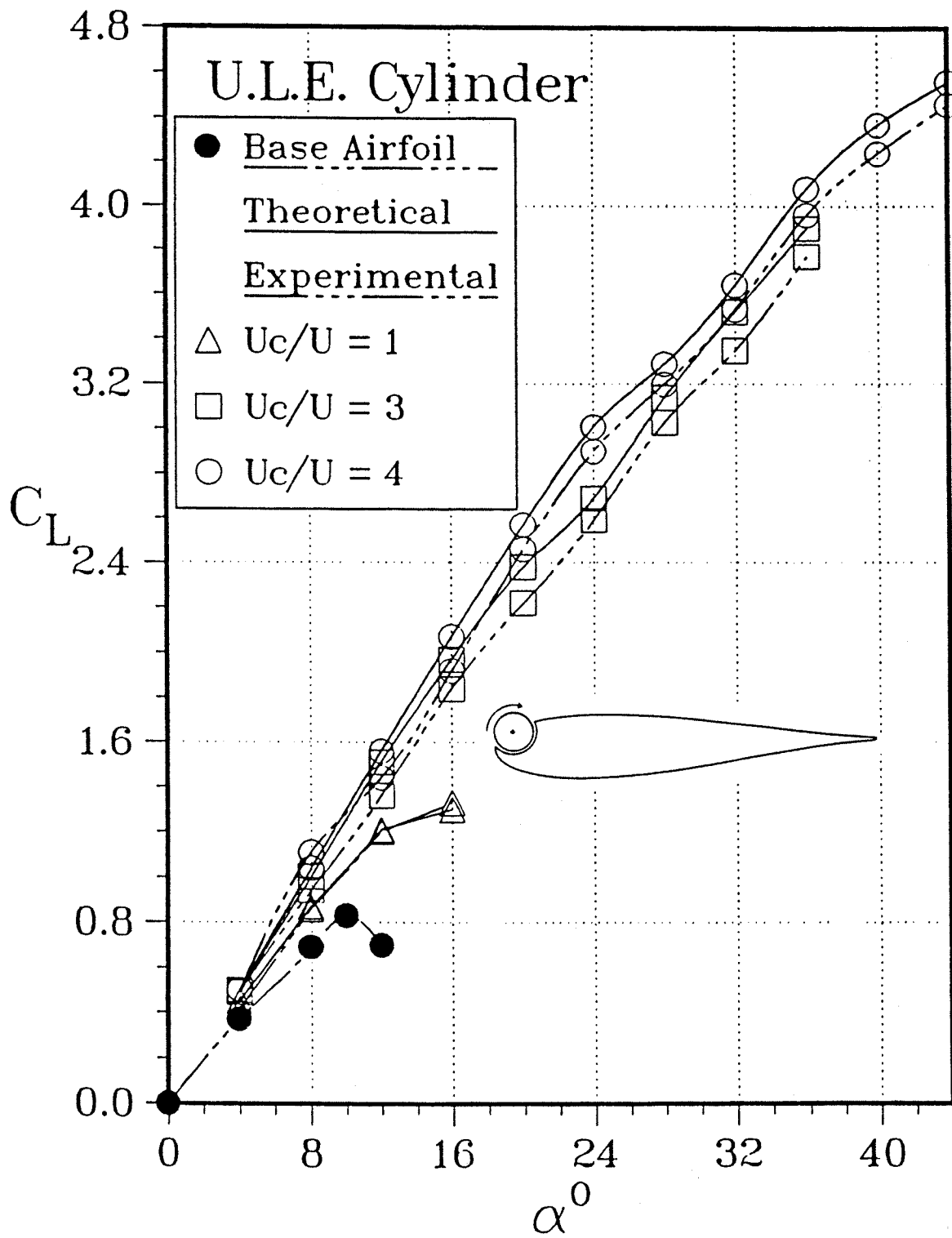
Figure 9    Lift and stall characteristics of the Joukowsky model as affected by the upper leading-edge cylinder rotation. Base airfoil ($U_c/U = 0$) data serve as reference to assess the effect of airfoil modification by the cylinder and its rotation.

advantage would be the mechanical simplicity of working with one cylinder.

## Comparative Performance

With a vast amount of data obtained through a planned experimental program using the configurations presented earlier, it would now be useful to compare their distinctive features to help establish relative merits. Figure 10 attempts to achieve this objective. Results of the standard Joukowsky airfoil (symmetrical, 15% thickness), with its $C_{L,\max} = 0.88$ and $\alpha_{stall} = 10°$, serve as reference for all the cases presented.

The leading-edge cylinder is quite effective in extending the lift curve, without significantly changing its slope, thus substantially increasing the maximum lift coefficient ($\approx 1.75$) and delaying the stall angle (28°). Further improvements in the maximum lift coefficient and stall angle are possible when the leading-edge cylinder is used in conjunction with an upper surface cylinder. This configuration also results in a lower drag due to a large recovery of pressure near the trailing edge, at moderately high angles of attack. The $C_{L,\max}$ realized with the leading-edge and forward upper-surface cylinders, was about 2.73 ($\alpha = 36°$), approximately three times that of the base configuration.

A rotating cylinder on the upper side of the leading edge also proves very effective. Although the maximum coefficient of lift realized with its rotation is slightly lower ($\approx 2.35$), it does have a major advantage in terms of mechanical simplicity. Note, now the lift curve has a lower slope and is not an extension of the base airfoil lift curve. Hence, the lift at a given $\alpha$ is relatively lower; however, the stall is delayed to around 48°.

On the other hand, to improve the lift over the range of low to medium angles of attack ($\alpha \leq 20°$), the trailing-edge cylinder proves much more effective, particularly in conjunction with the leading-edge cylinder. The suction over the airfoil upper surface as well as the compression on the lower surface are increased dramatically with the higher rates of rotation of this cylinder, resulting in a substantial increase in lift ($\approx 195\%$).

Thus, depending on the intended objective in terms of desired $C_{L,\max}$ and stall angle, one can select an appropriate configuration to initiate a preliminary design.

## Numerical Simulation

Simulation of fluid dynamical problems has been classically approached in two fundamentally different ways:
(a) modeling of the physical character of a phenomenon, as approached by Prandtl, through insight into the physics of the problem;

(b) simulation of the governing equations of motion as accomplished through finite element or finite difference schemes.

As can be expected each has its advantages and limitations. Here both the procedures are used to study the complex problem of a multielement airfoil with momentum injection using:
(a) the classical panel method;
(b) the surface singularity distribution with boundary-layer corrections;
(c) the finite element integration of the Navier-Stokes equations.

## Panel Method

The precise numerical solution of this complex problem involving moving boundaries can be obtained by solving the general time-dependent Navier-Stokes equations incorporating a suitable turbulence model. However, for realistic values of the Reynolds number, this would demand enormous computational effort and cost. On the other hand, judicious modelling of the flow character can provide information of sufficient accuracy for all engineering design purposes with nominal computational tools and insignificant cost. To that end, extension of the well developed panel code to multielement systems with momentum injection appeared quite attractive.

During the past three decades, the classical panel method involving distribution of surface-singularities has evolved to a sophisticated level where it can tackle complex geometries and flow separation condition[15-17]. Maskew and Dvorak[15] modelled separated flow by 'free-vortex lines' having a known constant vorticity but initially of unknown shape. Successive iterations yield the converged wake shape. Ribaut [16] accounted for the vorticity dispersion through dissipation and diffusion leading to a finite wake. The first-order panel method employing linearly varying vorticity along each panel and incorporating dispersion in the wake to model the separated flow[17] is also attractive.

In the present study of the multielement system, represented by an airfoil with the momentum
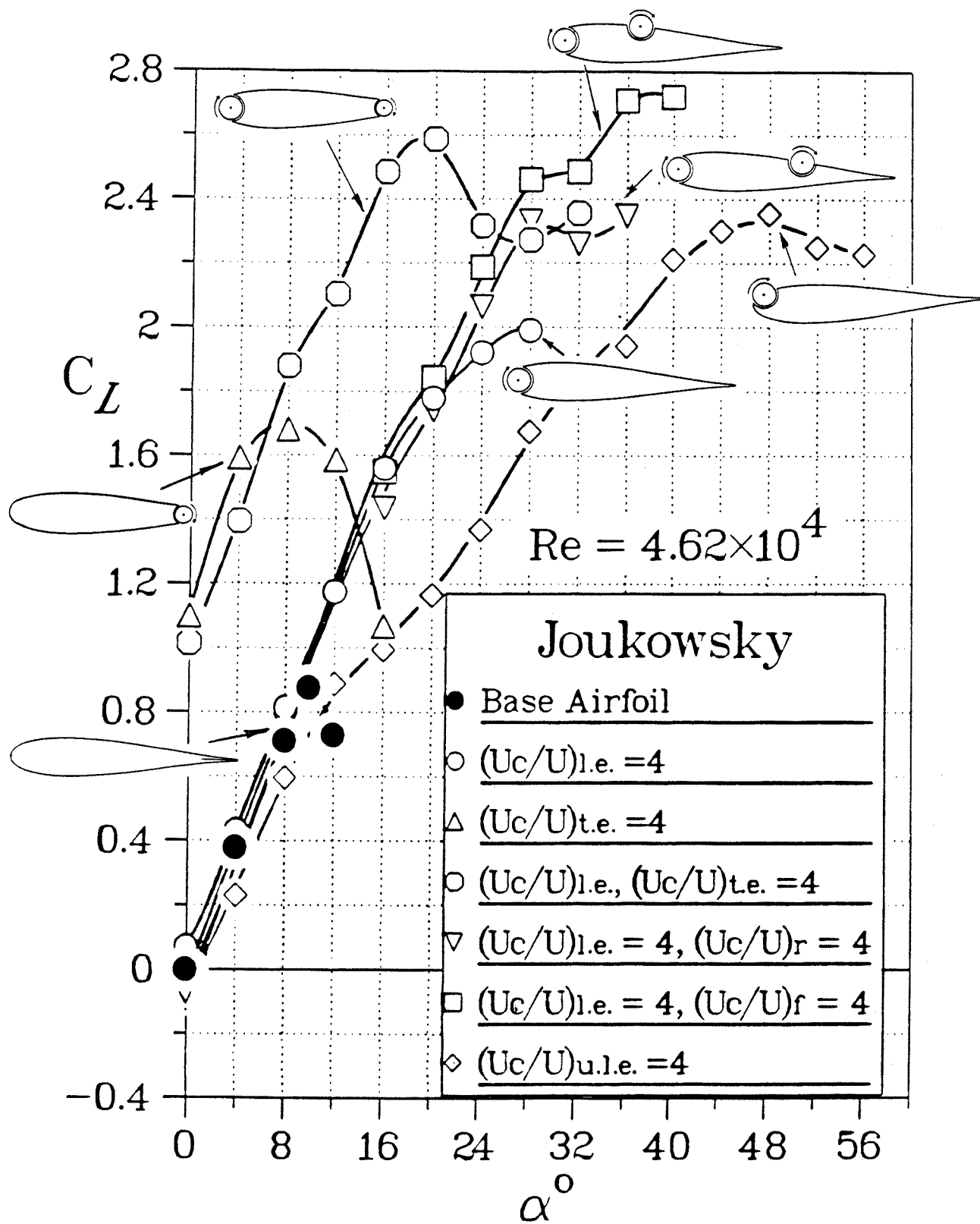
90

Figure 10    Plots to assess relative influence of different configuration studied on the lift and stall characteristics.

injecting rotating cylinder(s), each of the elements is represented by a large number of panels (100-150). Each panel has a continuous distribution of linearly varying vorticity and a constant source strength. The separated flow is modelled by the 'free-vortex lines' emanating from the lower and upper separation points. The free-vortex lines are also discretized into panels (Figure 11). At the beginning of the free-vortex line, the vorticity strength is taken to be equal to that at the separation point. The vorticity is allowed to dissipate at a given rate along the free-vortex lines resulting in a finite wake. An iterative scheme leads to the final solution.

Figure 12(a) compares numerically obtained surface pressure distribution on a two-dimensional Joukowsky airfoil with that measured during the wind tunnel tests for both without and with momentum injection. Note, even for such a complex multielement configuration with momentum injection the correlation is remarkably good. Figure 12(b) shows variation of the lift coefficient $C_L$ with $\alpha$, the angle of attack, as obtained through integration of the pressure distribution results obtained over a range of the angle of attack. Note, the panel method predicts the results with considerable accuracy sufficient for all practical design applications. A change in $C_{L,max}$ from 0.72 at $U_c/U = 0$ to 1.85 for $U_c/U = 4$ represents an increase of more than 150%. The corresponding delay in stall from 10° to 44° is remarkable and suggests promising V/STOL application.

Surface Singularity Distribution with Viscous Correction

The procedure here is similar to the one explained above, however, now the boundary-layer correction is applied. It is based on the surface singularity approach described in detail by Mokhtarian in his Ph.D. dissertation[7]. It accounts for the wall confinement and involves replacement of the airfoil and wind tunnel walls with vorticity distribution $\gamma$ in conjunction with appropriate constraint relations (Figure 13). Inclusion of a source within the contour of the airfoil models the wake when there is flow separation from the surface.

A finite difference boundary-layer scheme is used to introduce viscous corrections. The scheme employs potential flow pressure distribution results to calculate the boundary-layer characteristics at the top and bottom surfaces starting from the stagnation point until the point of separation.

The procedure uses the displacement thickness to construct an equivalent airfoil and then iterates

between the potential flow and boundary-layer scheme to converge to the final pressure distribution (Figure 14). Thus the objective is to match the outer potential flow solution with the inner boundary-layer prediction. The thin shear layer approximations of the Navier-Stokes equations for steady, two-dimensional, incompressible flow are used. The finite difference method employed for viscous correction is due to Keller and Cebeci[18,19]. The eddy viscosity term is expressed as suggested by Cebeci and Smith [20] which treats the turbulent boundary-layer as a composite layer consisting of inner and outer regions with separate expressions for eddy viscosity in each region. The details of the formulation and the finite difference procedure followed are those given by Cebeci and Bradshaw [21].

Typical results for the Joukowski airfoil with upper leading edge cylinder are presented in Figure 15. Wind tunnel test results are also included to facilitate comparison. As the numerical approach is able to account for the wall confinement effect, both the sets of data are corrected for blockage. Considering the complex character of the flow, the correlation is indeed excellent and the results can be used with confidence.

Finite Element Navier-Stokes Solution

Here the stream function-vorticity form of the Navier-Stokes equations are used in conjunction with the variable grid-size ($\approx 3000$ nodes, Figure 16) finite element analysis. Such a numerical solution of the two and three element airfoils with momentum injection is also not reported in the literature. The parametric analysis involving a systematic variation of the speed ratio, angle of attack and the Reynolds number gave detailed information about the pressure loading, separation condition and the time dependent wake (Figure 17). It also showed, rather spectacularly, effectiveness of the MSBC.

Figure 18 captures variation in the flow-field as the injected momentum is progressively increased through rotation of the cylinders from $U_c/U = 0$ to $U_c/U = 2$. The flow over the airfoil distinctly tends towards the potential character. The same trend can be observed through the spatial variation of the velocity vectors as shown in Figure 19 ($U_c/U = 4$).

Flow Visualization

To get better appreciation as to the physical character of the complex flow field as affected by the angle of attack and momentum injection parameters, extensive flow visualization study was undertaken. It also gave useful information about relative importance of the various system parameters and hence assisted in
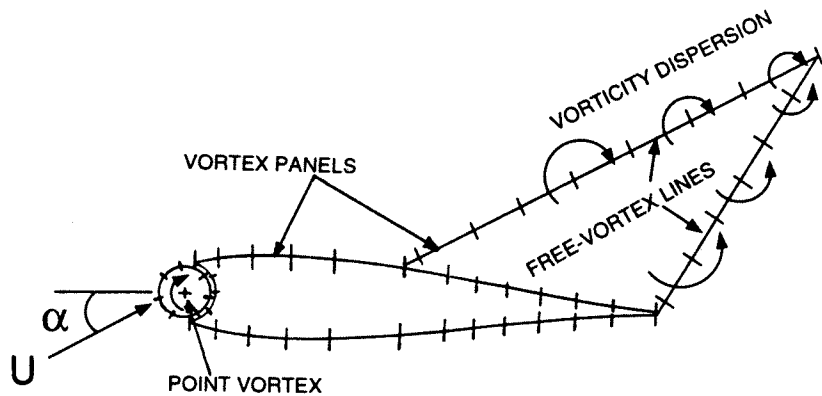
Figure 11    Classical panel method approach as applied to a symmetrical airfoil with the leading edge replaced by a rotating element for MSBC.
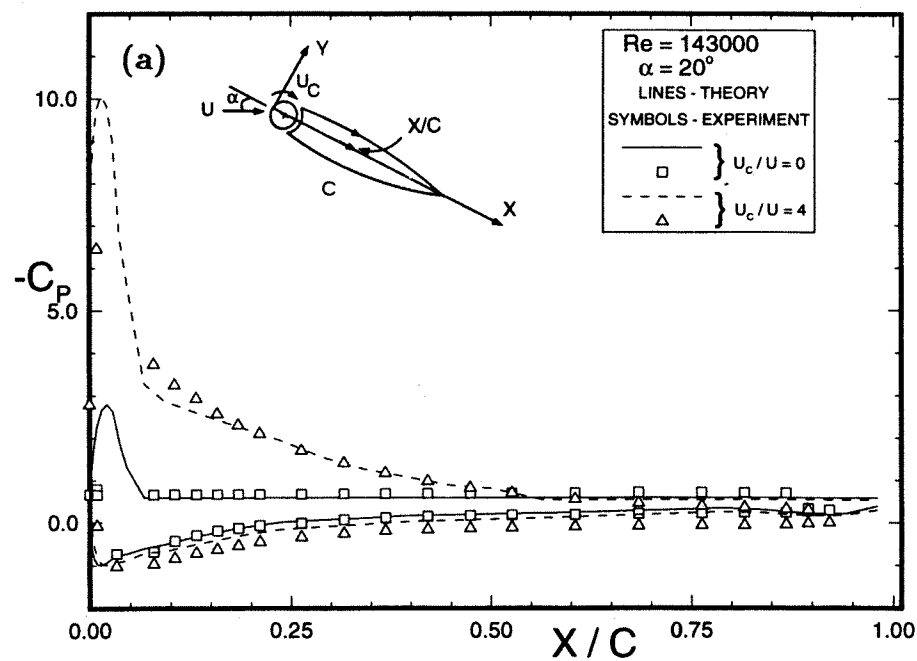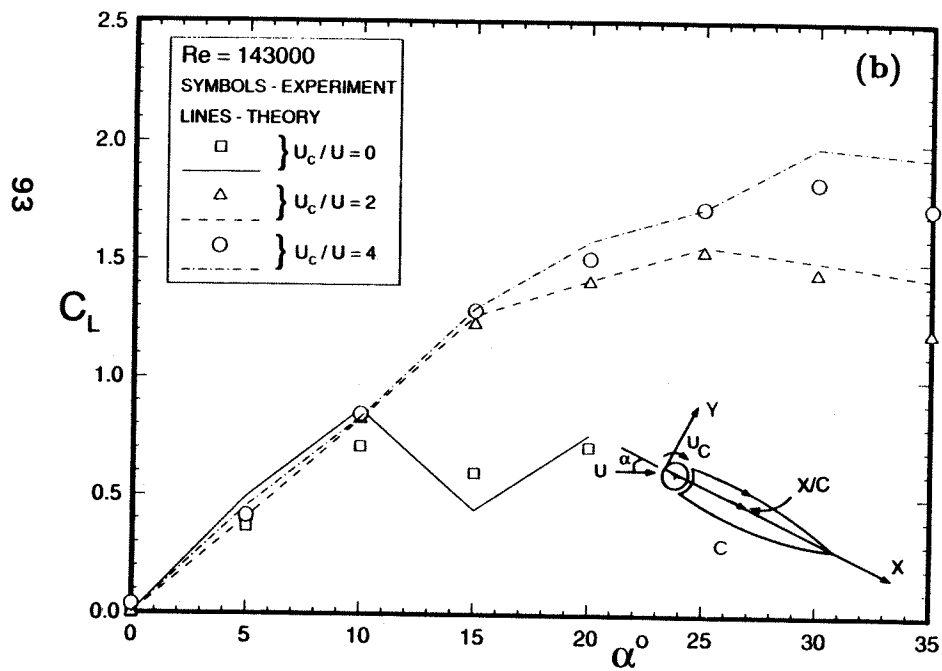


Figure 12    Comparison of the numerically obtained results with the experimental data for a Joukowski airfoil with the MSBC: (a) pressure distribution at α=20°; (b) variation of the lift co-efficient with angle of attack.

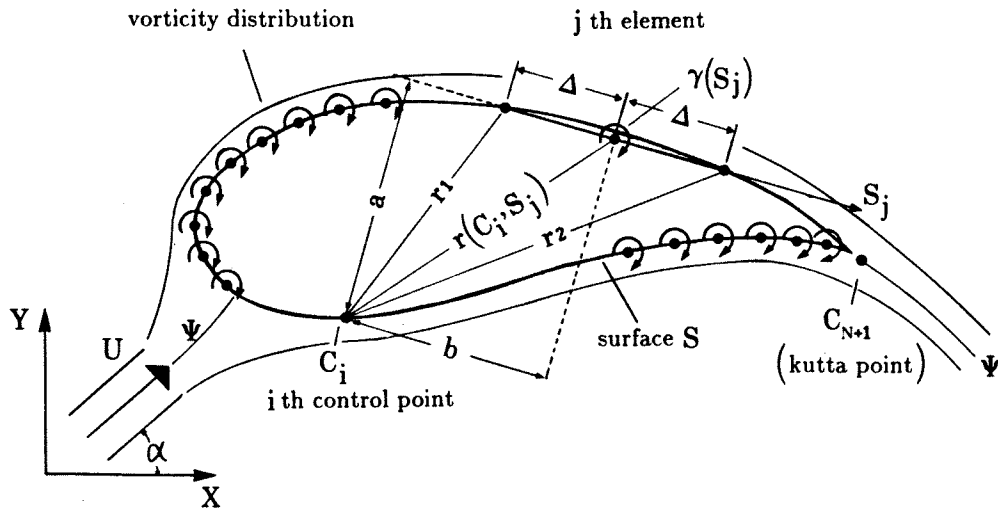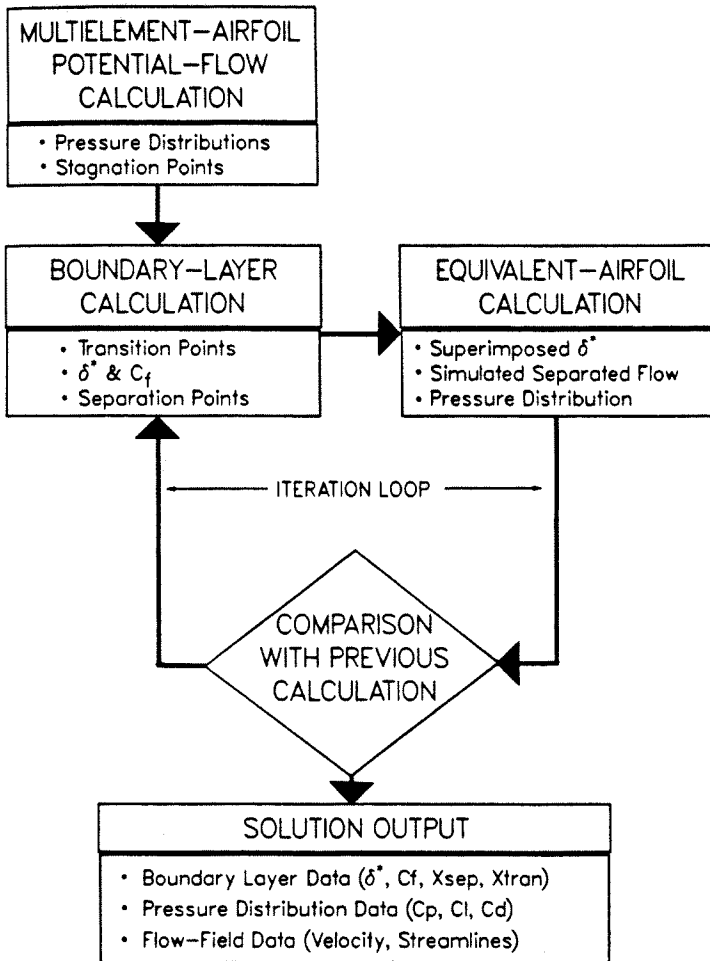Figure 13    Singularity representation of the airfoil and the notation for calculation of influence coefficients.



Figure 14    Flow chart for the numerical algorithm used for the viscous correction used in the surface singularity method: $\delta^*$, boundary-layer displacement thickness; $C_f$, local skin friction coefficient; $x_{sep}$, downstream location of the transition.
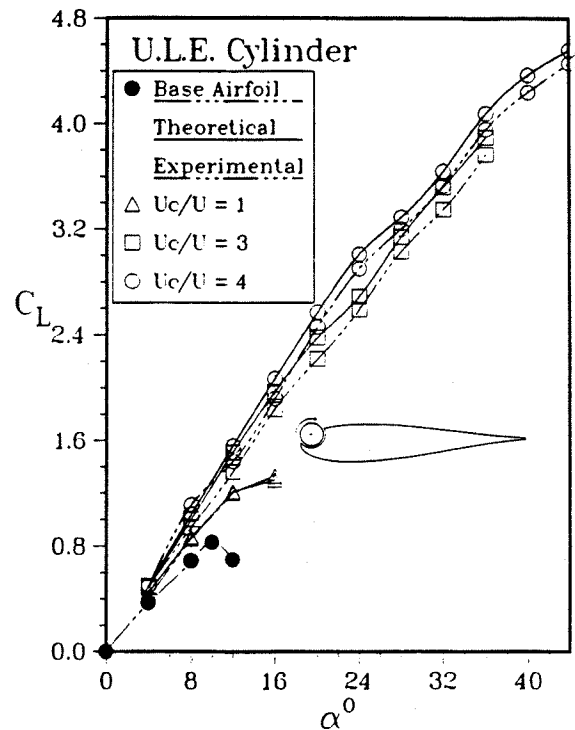
Figure 15    Variation of lift with angle of attack in presence of the MSBC as predicted by numerical and experimental procedures. Note, in spite of the complex character of the flow the correlation is excellent.
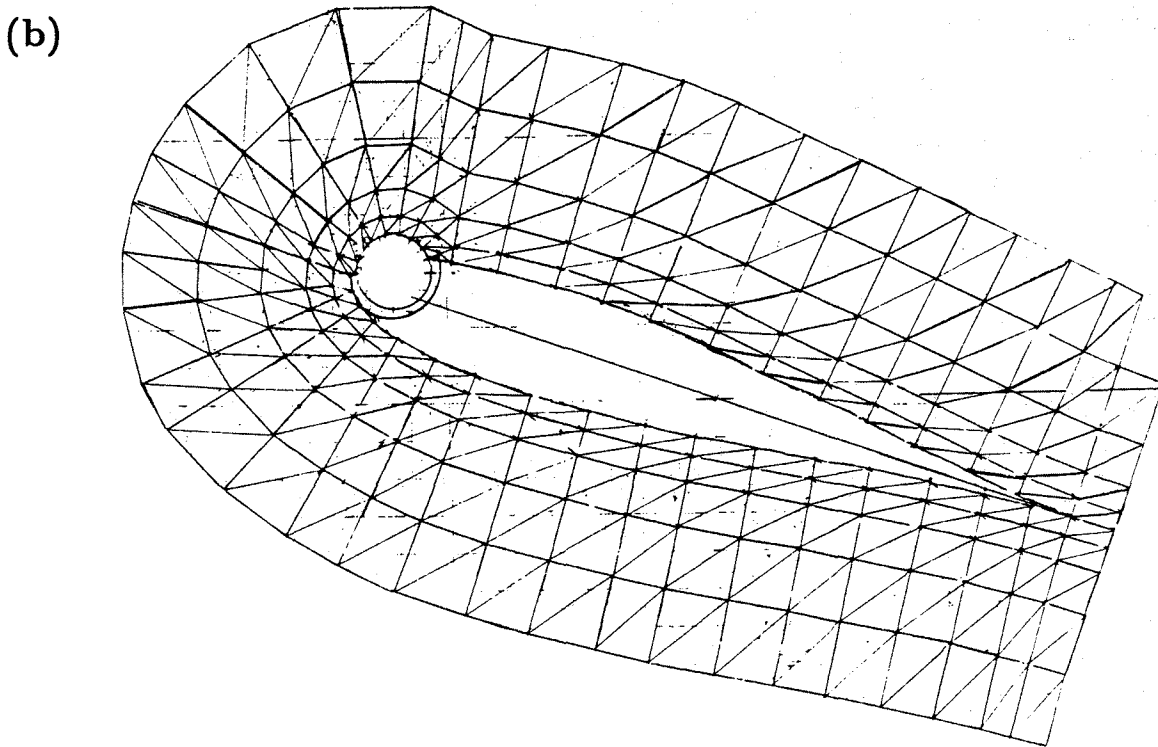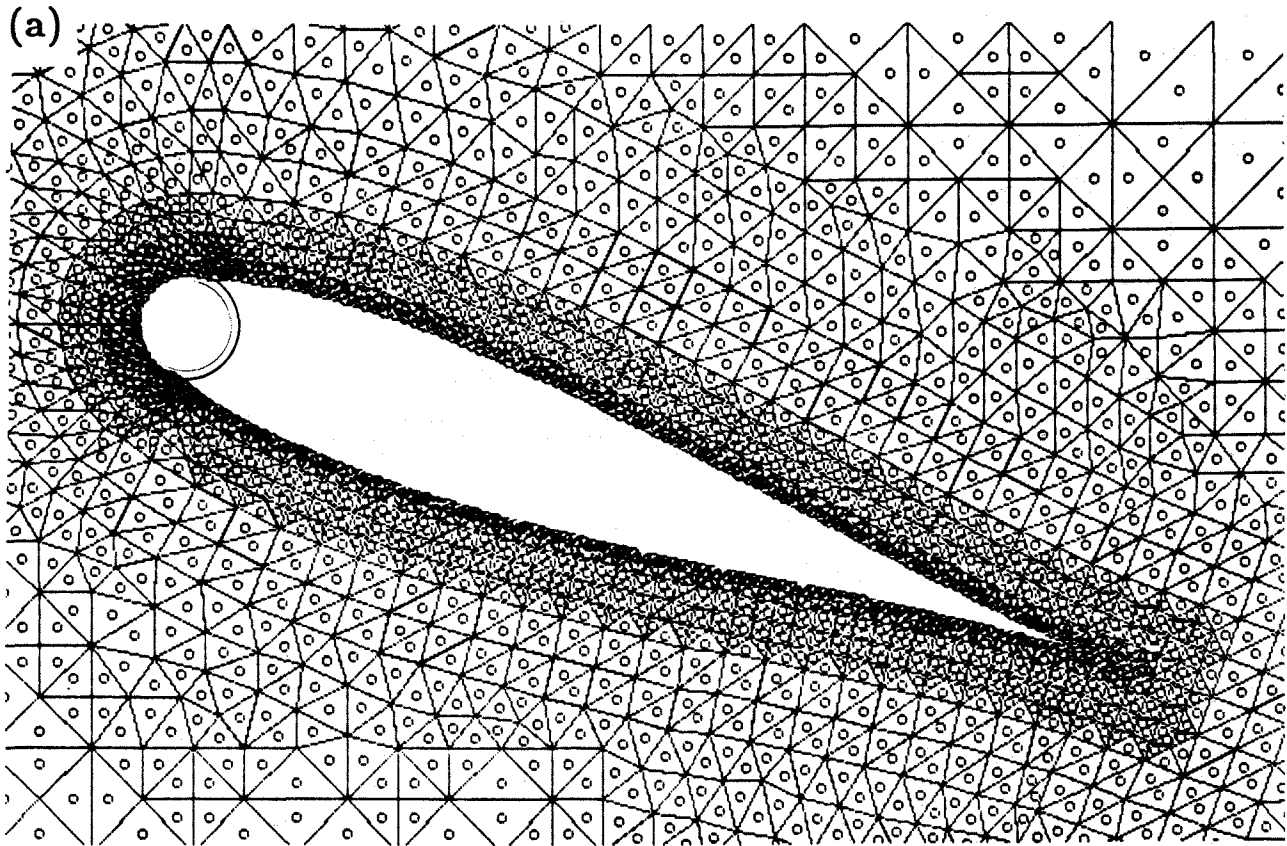
Figure 16    Triangular elements with spatially varying grid size used in the numerical simulation: (a) airfoil with the leading edge cylinder; (b) details of the mesh near the cylinder and airfoil surface for the upper leading edge configuration.
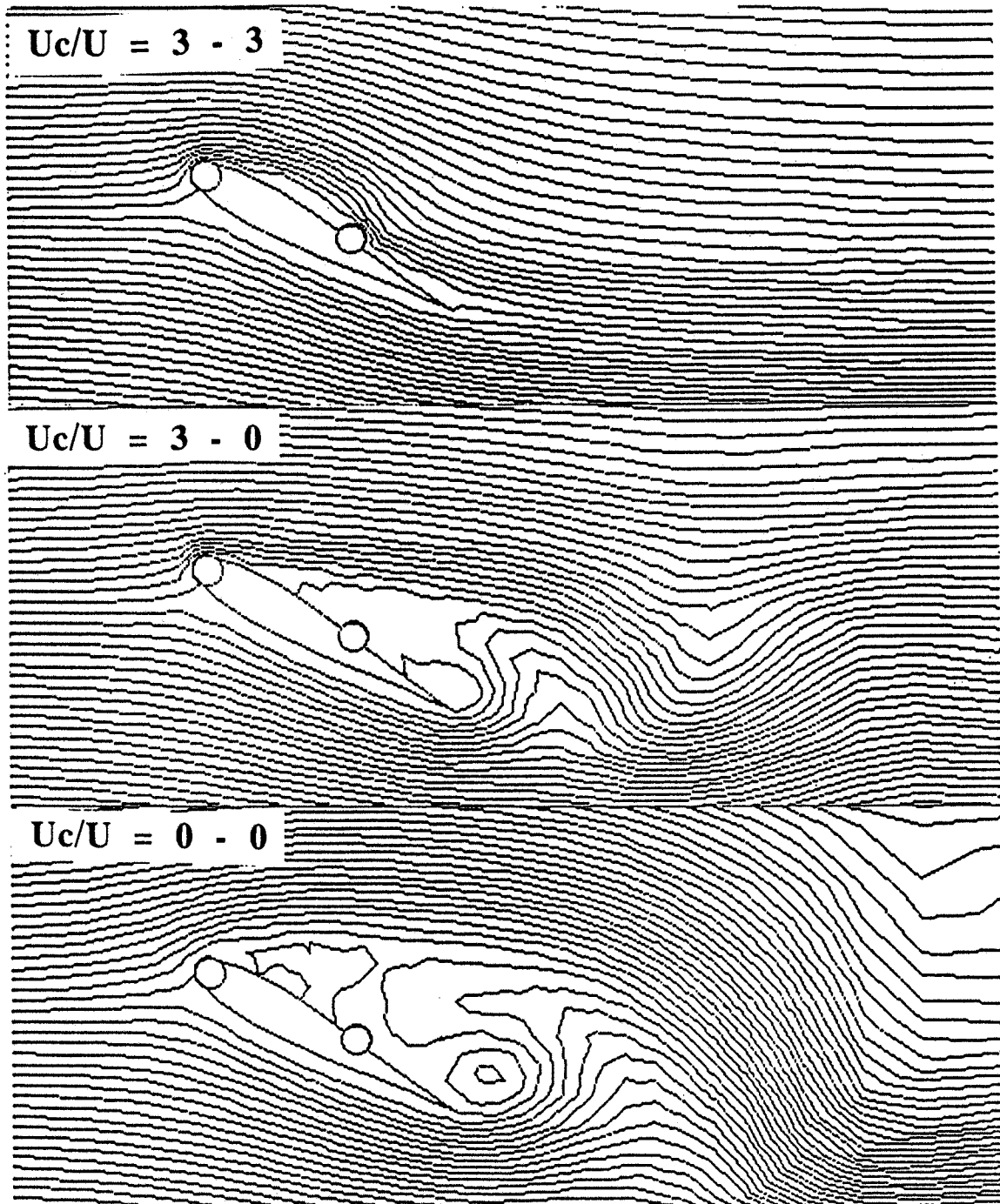
Figure 17    Finite element analysis showing the effect additional momentum injection due to introduction of the top
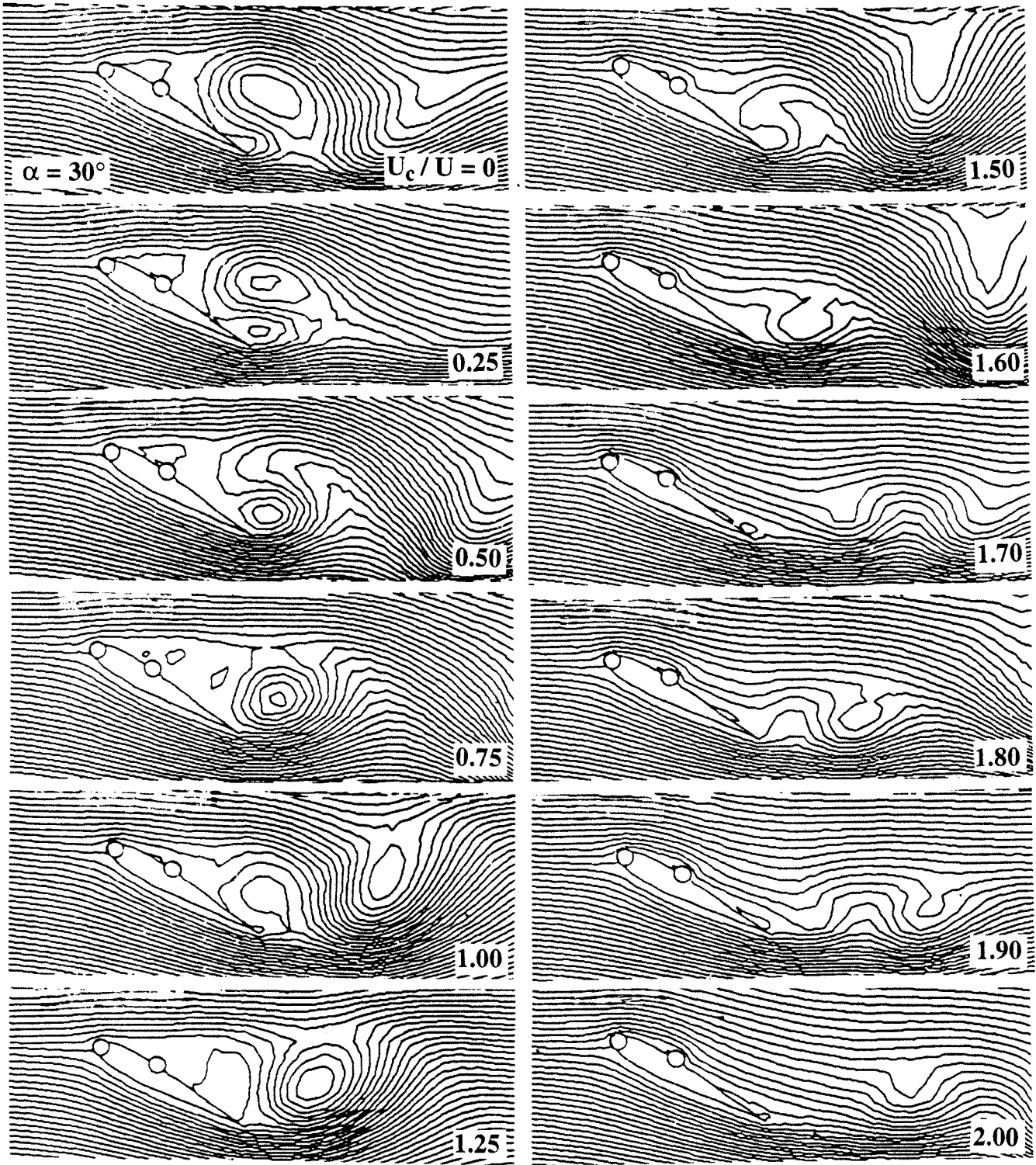surface cylinder, α = 30°. The results compared well with wind tunnel data and the flow visualization
study.

Figure 18    Variation in the flow-field as affected by progressive increase in the injected momentum. Note, the field tends to approach the potential character. Flow visualization confirmed this behaviour. The streamlines were obtained using the finite element integration of the Navier-Stokes equations.
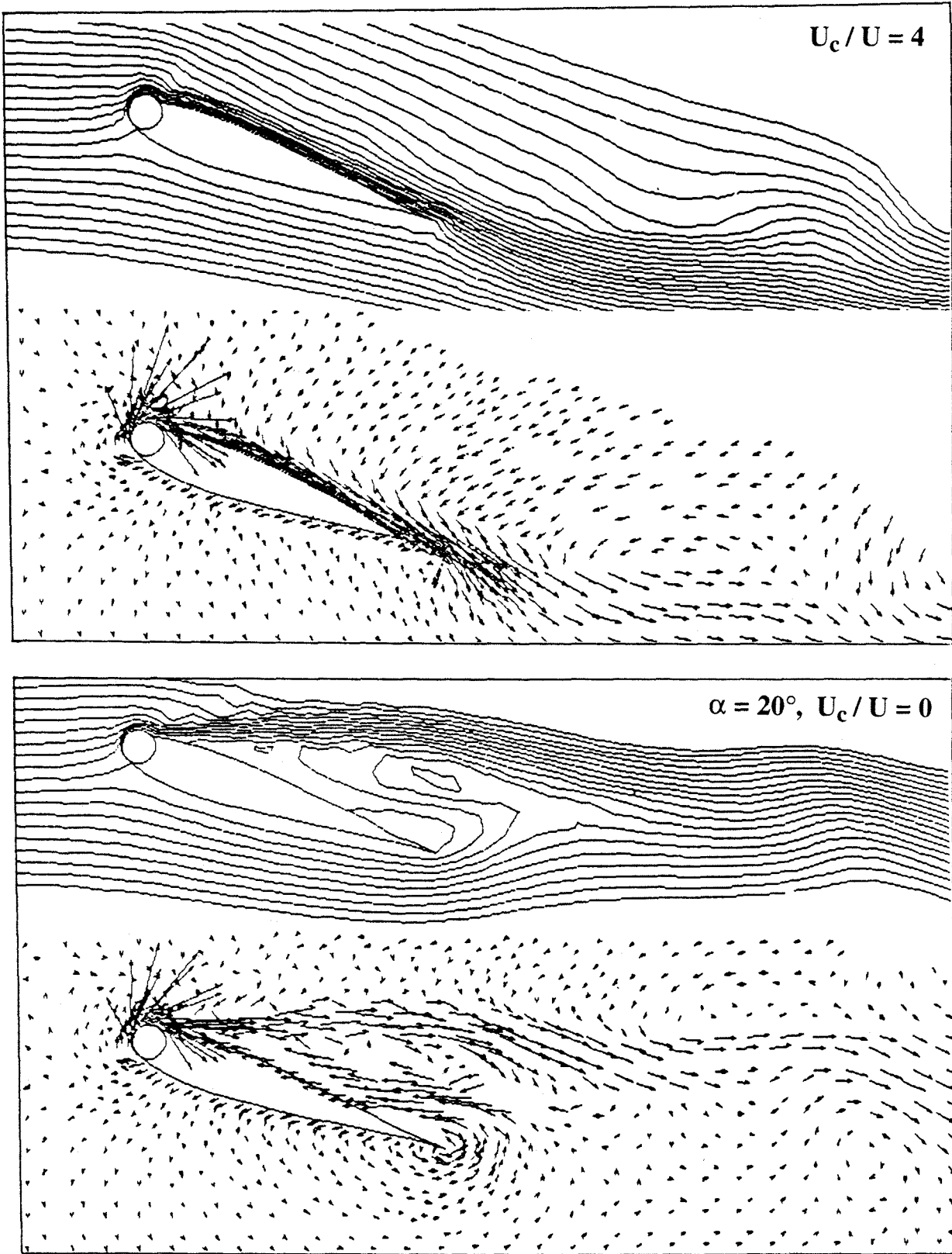
$U_c / U = 4$

$\alpha = 20°, \ U_c / U = 0$

Figure 19    Fluid flow-field and velocity distribution as given by the numerical finite element study of a multielement airfoil with momentum injection at $\alpha = 20°$.

planning of the experiments as well as the numerical analysis. The flow visualization tests were carried out in a closed circuit water channel facility (Figure 20). The models were constructed from Plexiglas and fitted with rotating cylinders driven by variable speed d.c. motors. A suspension of fine polyvinyl chloride powder was used in conjunction with slit lighting to visualize streaklines. Both angle of attack and cylinder speeds were systematically changed and still photographs as well as video movies were taken.

The study showed, rather dramatically, effectiveness of this form of boundary-layer control (Figure 21). With the leading-edge cylinder model at $\alpha = 20°$ and in absence of the cylinder rotation, a well-defined early separation resulting in a wide wake is quite apparent, with large-scale vortices sweeping away downstream. However, with the cylinder rotating at $U_c/U = 4$, an essentially attached flow is established over the most of the upper surface of the airfoil, even at such a high angle of attack, considerably beyond the nominal stall angle of around 10°. Even for the angle of attack of 30°, the MSBC continued to be effective as shown in Figure 22 for the airfoil with the cylinder located at the upper leading edge. The large angle of attack and the leading edge geometry leads to only a small cylinder surface exposed to the fluid stream. Hence, the cylinder rotation speed has to be relatively high to inject necessary momentum for the boundary-layer control.

At relatively lower rates of cylinder rotation, the flow character was found to be similar to that observed at $U_c/U = 1$, with the separation and reattachment regions progressively shifting downstream as the rotation rate increased. This is apparent through a progressive increase in $U_c/U$ from 0 to 4. In fact, the flow pattern was found to be quite unsteady with the vortex layer separating and forming a bubble on reattachment, the whole structure drifting downstream, diffusing, and regrouping at different scales of vortices. Ultimately the flow sheds large as well as small vortices. This unsteady character of the separating shear layer and the wake is clearly evident in the video. Thus the flow character indicated by the experimentally obtained time-averaged plots appears to be a fair description of the process.

## Concluding Remarks

Based on the wind tunnel tests, complemented by numerical and flow visualization studies, the following general comments can be made:

(i)   The Moving Surface Boundary-Layer Control (MSBC) can significantly increase lift, decrease drag and delay stall of aircraft. Its application to the next generation of high performance airplanes is indeed quite exciting.

(ii)  The concept is essentially semi-passive in character requiring negligible amount of power for its implementation. This makes it quite attractive for real-life application. During the wind tunnel tests, the peak power required was around 90W.

(iii) Numerical approach to the problem, even using the rather simple panel approach, can provide useful results of sufficient accuracy for preliminary design purposes. This is remarkable considering highly complex character of the flow and suggests significant saving in time, effort and computational cost.

(iv)  The more elaborate finite element method is able to predict character of the flow field with considerable accuracy.

(v)   Flow visualization study confirms effectiveness of the MSBC quite dramatically.

(vi)  The concept of MSBC presents several avenues of promising applications which are under study. They include performance improvement of a delta wing and its control surfaces; drag reduction of bluff bodies such as tractor-trailer truck configuration; and suppression of vortex resonance and galloping type of wind induced instabilities .

## References

1.   Goldstein, S., *Modern Developments in Fluid Mechanics,* Vol. I and II, Oxford University Press, 1938.

2.   Lachmann, G.V., *Boundary Layer and Flow Control,* Vol. I and II, Pergamon Press, 1961.

3.   Rosenhead, L., *Laminar Boundary Layers,* Oxford University Press, 1966.

4.   Schlichting, H., *Boundary-Layer Theory,* McGraw-Hill Book Company, 1968.

5.   Chang, P.K., *Separation of Flow,* Pergamon Press, 1970.

6.   Tennant, J.S., Johnson, W.S., and Krothapalli, A., "Rotating Cylinder for Circulation Control on

an Airfoil", *Journal of Hydronautics*, Vol. 10, No. 3, July 1976, pp. 102-105.

7. Mokhtarian, F., *Fluid Dynamics of Airfoils with Moving Surface Boundary-Layer Control*, Ph.D. Thesis, University of British Columbia, February 1988.

8. Modi, V.J., Ying, B., and Yokomizo, T., "Boundary-layer Control of Bluff Bodies through Momentum Injection", *SAE Transactions, Journal of Commercial Vehicles*, Section 2, Vol. 99, 1991, pp. 778-794.

9. Modi, V.J., and Yokomizo, T., "On the Boundary-layer Control Through Momentum Injection", *The Sabita Chaudhury Memorial Lecture, Proceedings of the International Symposium on Aerospace Sciences and Engineering*, Bangalore, India, December 1992, Editor: H.S. Mukunda, McGraw-Hill Publisher, in press ; also *Sadhana, the Proceedings of the Indian Academy of Sciences*, in press.

10. Favre, A., "Contribution a L'etude Experimentale des Mouvement Hydrodynamiques a Deux Dimensions", Thesis presented to the *University of Paris*, 1938.

11. Alvarez-Calderon, A., and Arnold, F.R., "A Study of the Aerodynamic Characteristics of a High Lift Device Based on Rotating Cylinder Flap", *Stanford University Technical Report RCF-1*, 1961.

12. Cichy, D.R., Harris, J.W., and MacKay, J.K., "Flight Tests of a Rotating Cylinder Flap on a North American Rockwell YOV-10A Aircraft", *NASA* CR-2135, November 1972.

13. Weiberg, J.A., Giulianetti, D., Gambucci, B., and Innis, R.C., "Takeoff and Landing Performance and Noise Characteristics of a Deflected STOL Airplane with Interconnected Propellers and Rotating Cylinder Flaps", *NASA* TM X-62, 320, December 1973.

14. Cook, W.L., Mickey, D.M., and Quigley, H.G., "Aerodynamics of Jet Flap and Rotating Cylinder Flap STOL Concepts", *AGARD Fluid Dynamics Panel Symposium on V/STOL Aerodynamics*, Delft, Netherlands, April 24-26, 1974, Paper No. 10.

15. Maskew, B., and Dvorak, F.A., "The Prediction of $C_{Lmax}$ Using a Separated Flow Model," *Journal of American Helicopter Society*, Vol. 23, April 1978, pp. 2-8.

16. Ribaut, M., "A Vortex Sheet Method for Calculating Separated Two-dimensional Flows," *AIAA Journal*, Vol. 21, August 1983, pp. 1079-1084.

17. Mukherjea, S., and Bandyopadhyay, G., "Separated Flow about a Wedge," *The Aeronautical Journal of the Royal Aeronautical Society*, June-July 1990, pp. 196-202.

18. Keller, H.B. and Cebeci, T., "Accurate Numerical Methods for Boundary-Layer Flows, Part 1, Two-Dimensional Laminar Flows", *Lecture Notes in Physics, 8, Proceedings of the Second International Conference on Numerical Methods in Fluid Dynamics*, p. 92, Springer-Verlag, New York, 1971.

19. Keller, H.B., and Cebeci, T., "Accurate Numerical Methods for Boundary-Layer Flows, Part 2, Two-Dimensional Turbulent Flows", *AIAA Journal*, Vol. 10, p. 1193, 1972.

20. Cebeci, T., and Smith, A.M.O., *Analysis of Turbulent Boundary Layers*, Academic Press, New York, 1974.

21. Cebeci, T., and Bradshaw, P., *Momentum Transfer in Boundary Layers*, Hemisphere-McGraw Hill, Washington, 1977

MIRROR   SOURCE OF LIGHT  SLIT

SHEET LIGHT

MODEL

500   130      2630

HONEYCOMB

PUMP
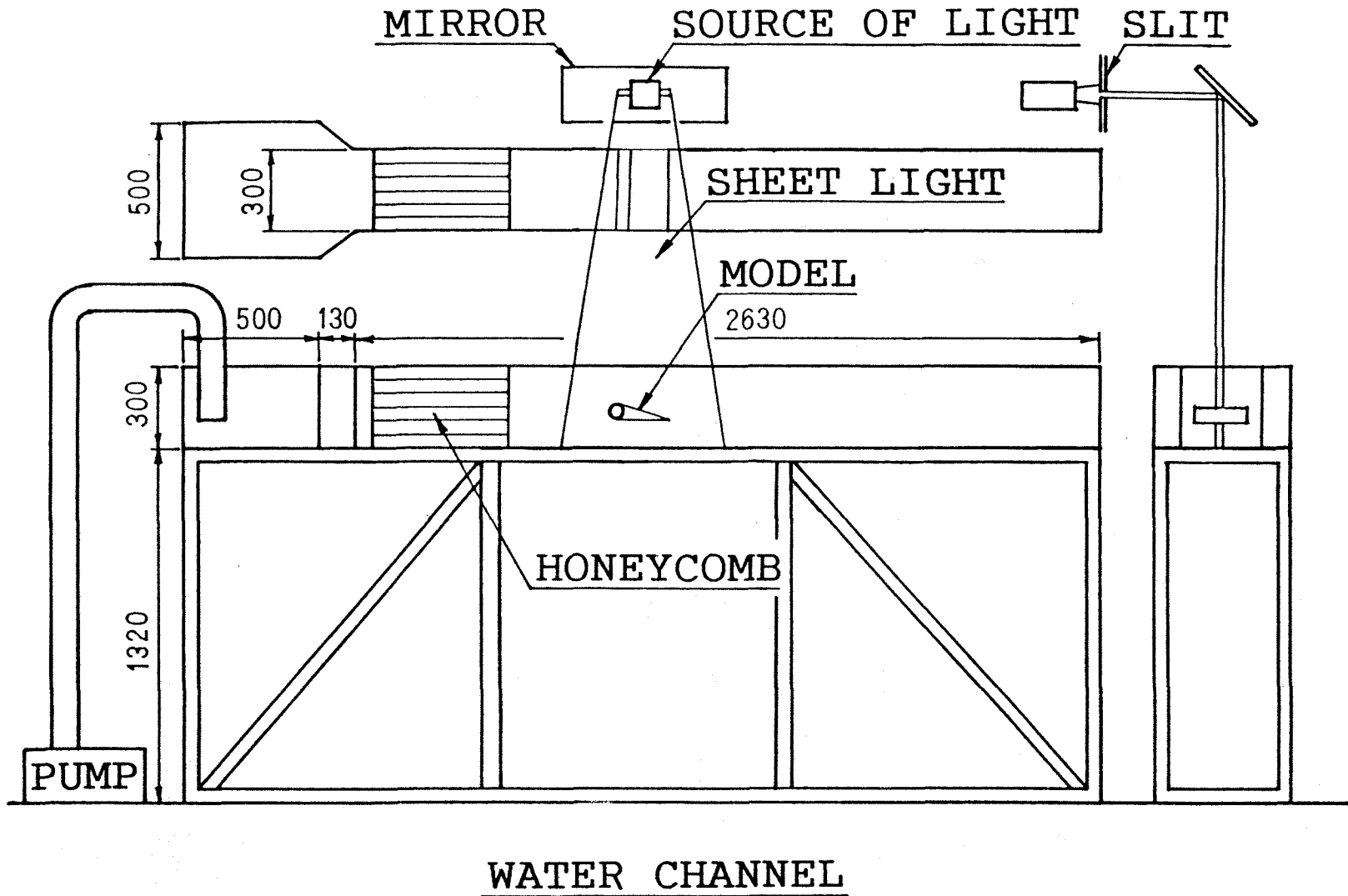
## WATER CHANNEL

Figure 20   A schematic diagram of the closed circuit water channel facility used in the flow visualization study. Slit lighting was used to minimize distortion due to three dimensional character of the flow. Long exposure provided path-lines with polyvinyl chloride particles serving as tracers. The dimensions are in mm.
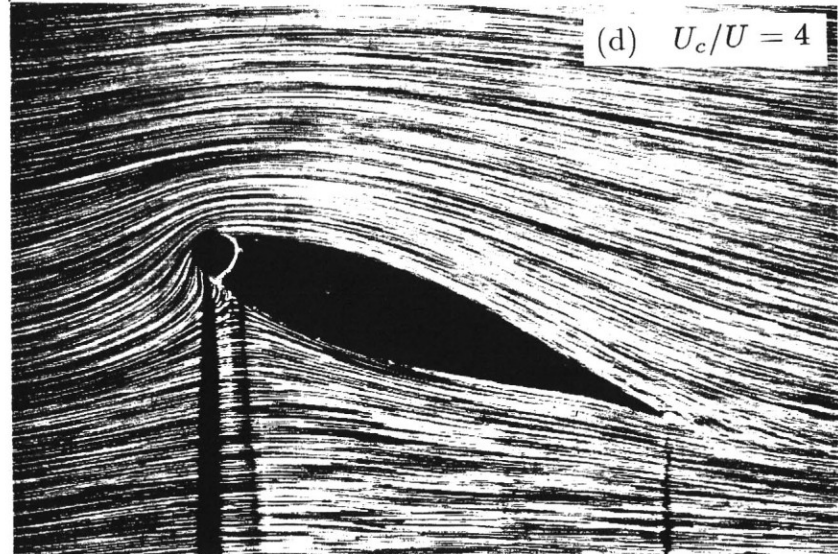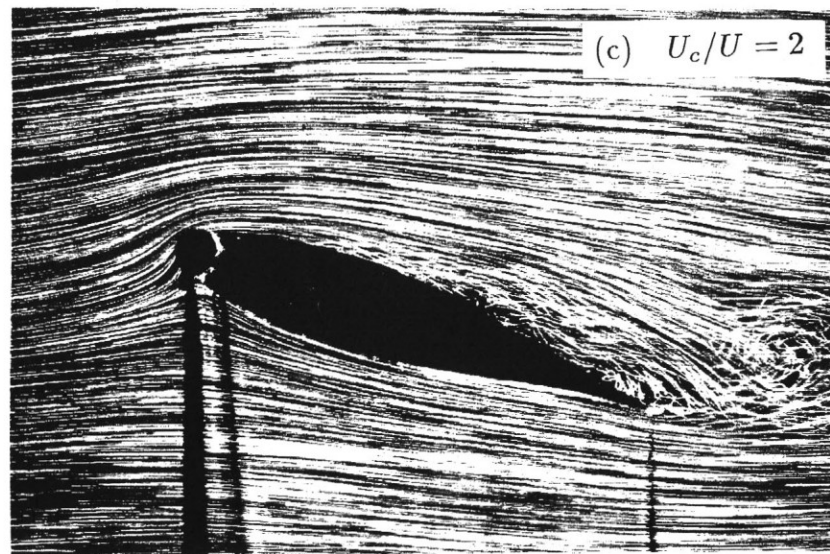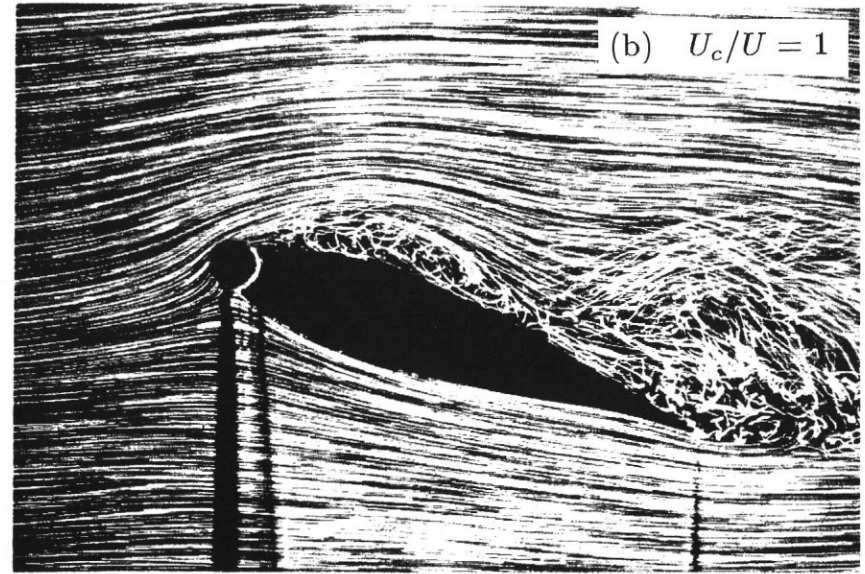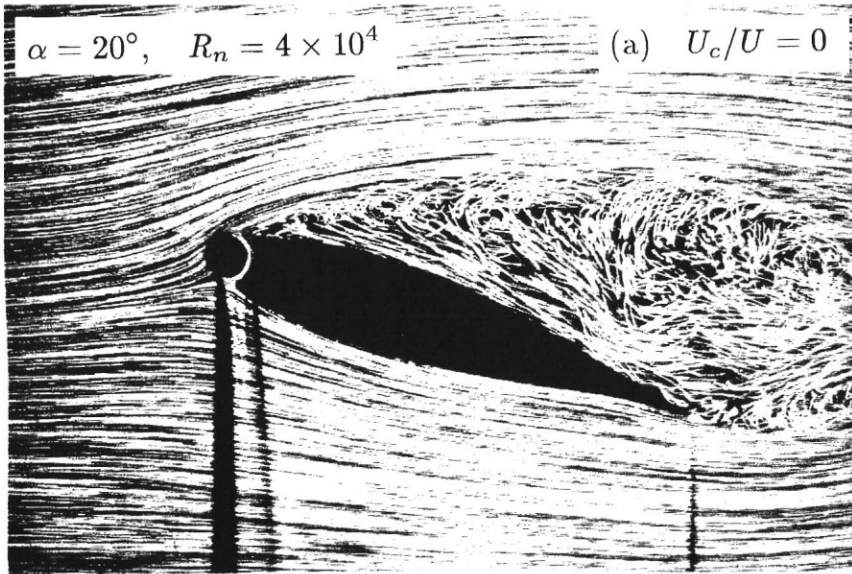
Figure 21 Representative flow visualization pictures, showing rather dramatically, successful control of the boundary-layer separation through momentum injection. Note the similarity with the numerically
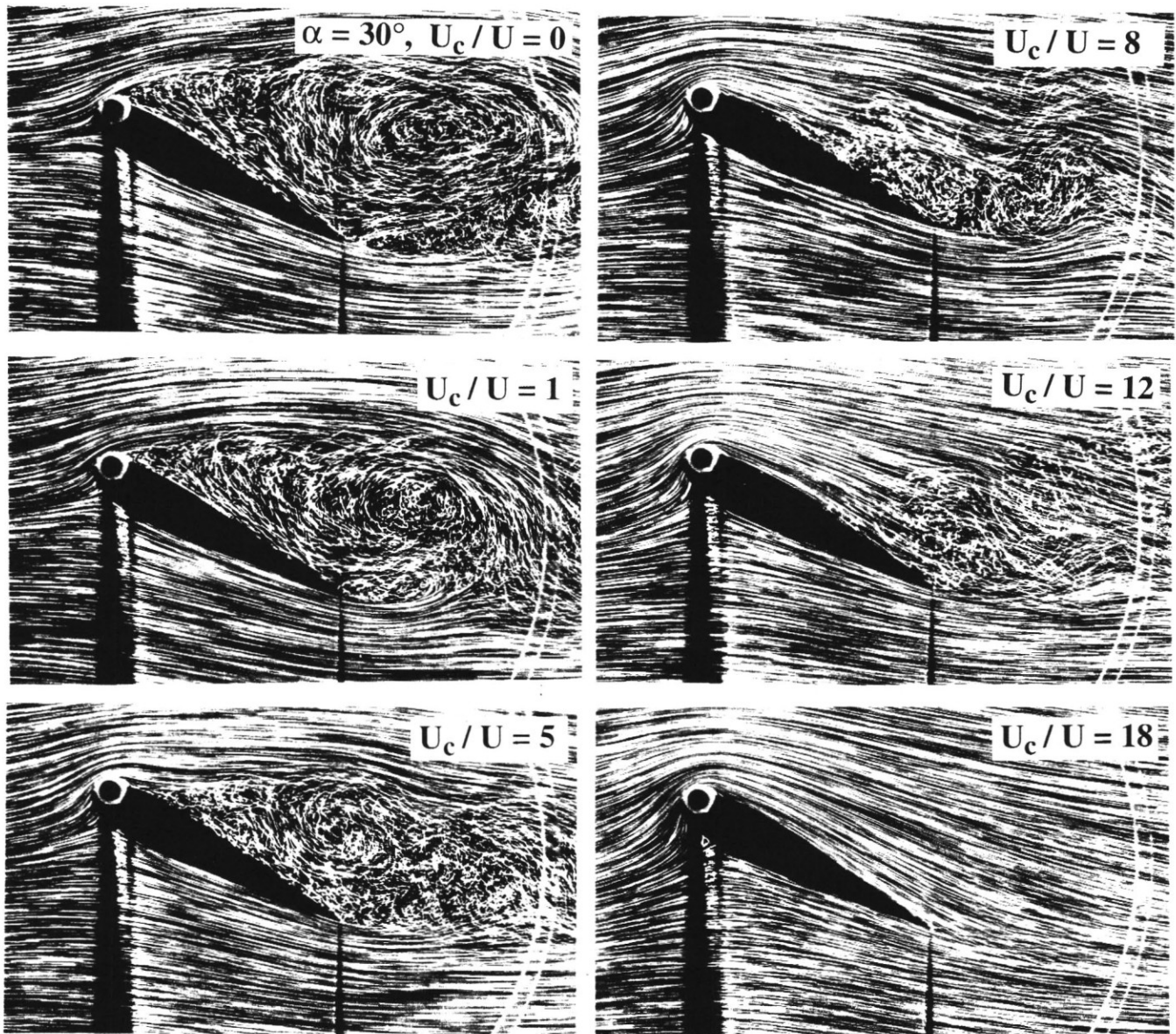
Figure 22    Flow visualization pictures for a symmetrical Joukowsky airfoil with upper leading edge cylinder. Note, the progressive downstream shift of the separation point with increase in the momentum injection culminating, essentially, in the potential flow at $U_c/U = 18$.